



**HAL**  
open science

**New line list for the  $\nu_4$  bands of the trans (790.117  $\text{cm}^{-1}$ ) and cis (851.943  $\text{cm}^{-1}$ ) conformers of nitrous acid (HONO): Accurate positions and absolute intensities**

A. Perrin, L. Manceron, J. Vander Auwera, Wilfried Tchana Betnga, Francis Hindle, Arnaud Cuisset, Gaël Mouret, Robin Bocquet, P. Roy, Xavier Landsheere, et al.

► **To cite this version:**

A. Perrin, L. Manceron, J. Vander Auwera, Wilfried Tchana Betnga, Francis Hindle, et al.. New line list for the  $\nu_4$  bands of the trans (790.117  $\text{cm}^{-1}$ ) and cis (851.943  $\text{cm}^{-1}$ ) conformers of nitrous acid (HONO): Accurate positions and absolute intensities. *Journal of Quantitative Spectroscopy and Radiative Transfer*, 2024, 325, pp.109082. 10.1016/j.jqsrt.2024.109082 . hal-04643183

**HAL Id: hal-04643183**

**<https://hal.science/hal-04643183v1>**

Submitted on 10 Jul 2024

**HAL** is a multi-disciplinary open access archive for the deposit and dissemination of scientific research documents, whether they are published or not. The documents may come from teaching and research institutions in France or abroad, or from public or private research centers.

L'archive ouverte pluridisciplinaire **HAL**, est destinée au dépôt et à la diffusion de documents scientifiques de niveau recherche, publiés ou non, émanant des établissements d'enseignement et de recherche français ou étrangers, des laboratoires publics ou privés.

## Journal Pre-proof

New line list for the  $\nu_4$  bands of the trans ( $790.117\text{ cm}^{-1}$ ) and cis ( $851.943\text{ cm}^{-1}$ ) conformers of nitrous acid (HONO): accurate positions and absolute intensities

W. Tchana Betnga , A. Perrin , L. Manceron , J. Vander Auwera ,  
F. Hindle , A. Cuisset , G. Mouret , R. Bocquet , P. Roy ,  
X. Landsheere , A. Voute , F. Kwabia Tchana

PII: S0022-4073(24)00189-4  
DOI: <https://doi.org/10.1016/j.jqsrt.2024.109082>  
Reference: JQSRT 109082



To appear in: *Journal of Quantitative Spectroscopy & Radiative Transfer*

Received date: 26 April 2024  
Revised date: 9 June 2024  
Accepted date: 10 June 2024

Please cite this article as: W. Tchana Betnga , A. Perrin , L. Manceron , J. Vander Auwera , F. Hindle , A. Cuisset , G. Mouret , R. Bocquet , P. Roy , X. Landsheere , A. Voute , F. Kwabia Tchana , New line list for the  $\nu_4$  bands of the trans ( $790.117\text{ cm}^{-1}$ ) and cis ( $851.943\text{ cm}^{-1}$ ) conformers of nitrous acid (HONO): accurate positions and absolute intensities, *Journal of Quantitative Spectroscopy & Radiative Transfer* (2024), doi: <https://doi.org/10.1016/j.jqsrt.2024.109082>

This is a PDF file of an article that has undergone enhancements after acceptance, such as the addition of a cover page and metadata, and formatting for readability, but it is not yet the definitive version of record. This version will undergo additional copyediting, typesetting and review before it is published in its final form, but we are providing this version to give early visibility of the article. Please note that, during the production process, errors may be discovered which could affect the content, and all legal disclaimers that apply to the journal pertain.

© 2024 Published by Elsevier Ltd.

**HIGHLIGHT**

- absolute line intensities for the  $\nu_4$  bands of Trans-HONO and Cis-HONO measured
- improved line positions using infrared FTS spectra on SOLEIL
- Line list for HONO in the 11  $\mu\text{m}$  infrared region
- For *cis*-HONO, the  $\{4^1, 5^1, 6^1\}$  energy levels are coupled together.

Journal Pre-proof

**New line list for the  $\nu_4$  bands of the *trans* (790.117  $\text{cm}^{-1}$ ) and *cis* (851.943  $\text{cm}^{-1}$ ) conformers of nitrous acid (HONO): accurate positions and absolute intensities**

W. Tchana Betnga<sup>1,2</sup>, A. Perrin<sup>3,\*</sup>, L. Manceron<sup>1,4</sup>, J. Vander Auwera<sup>5</sup>, F. Hindle<sup>2</sup>, A. Cuisset<sup>2</sup>, G. Mouret<sup>2</sup>, R. Bocquet<sup>2</sup>, P. Roy<sup>5</sup>, X. Landsheere<sup>1</sup>, A. Voute<sup>1,4</sup> and F. Kwabia Tchana<sup>1</sup>

<sup>1</sup> Université Paris Cité and Univ Paris Est Creteil, CNRS, LISA, F-75013 Paris, France

<sup>2</sup> Université du Littoral Côte d'Opale, UR 4493, Laboratoire de Physico-Chimie de l'Atmosphère, F-59140 Dunkerque, France

<sup>3</sup> Laboratoire de Météorologie Dynamique/IPSL, UMR CNRS 8539, Ecole Polytechnique, Université Paris-Saclay, RD36, 91128 Palaiseau Cedex, France

<sup>4</sup> Synchrotron SOLEIL, Ligne AILES, L'Orme des Merisiers, St-Aubin BP48, 91192 Gif-sur-Yvette Cedex, France

<sup>5</sup> Spectroscopy, Quantum Chemistry and Atmospheric Remote Sensing (SQUARES), C.P. 160/09, Université Libre de Bruxelles, 50 avenue F.D. Roosevelt, B-1050 Brussels, Belgium

\*Corresponding author: Agnès Perrin agnes.perrin@lmd.ipsl.fr

Nb of Tables: 9

Nb of Figures: 13

Keywords: *trans*-HONO, *cis*-HONO, 11  $\mu\text{m}$ , accurate positions, absolute intensities, GEISA, IASI-NG

## Abstract

The goal of this work was to update and significantly improve the line lists that have been generated recently for 11  $\mu\text{m}$  bands of the *trans*- and *cis*- conformer forms of nitrous acid (HONO) [Armante R, Perrin A, Kwabia Tchana F, Manceron L. The  $\nu_4$  bands at 11  $\mu\text{m}$ : linelists for the *trans*- and *cis*- conformer forms of nitrous acid (HONO) in the 2019 version of the GEISA database. *Molecular Physics* 2021;120:e1951860]. That 2019 version of the 11  $\mu\text{m}$  line list was generated using the spectroscopic parameters that were available, at that time, in the literature. During the present study, we used high-resolution Fourier transform spectra recorded at 11  $\mu\text{m}$  to perform a large investigation of line positions and intensities for the  $\nu_4$  bands of the *trans*- and *cis*-conformer of HONO. The resulting set of experimental  $\nu_4$  (absolute) intensities and of  $4^1$  energy levels were used to determine, by least squares fit computations, improved position and intensity parameters for the  $\nu_4$  bands of the *trans*- and *cis*-conformer of HONO. For *trans*-HONO, the  $\nu_4$  band appeared not to be perturbed, while for *cis*-HONO a weak high order B-type Coriolis, coupling together the  $4^1$  and  $6^1$  energy levels was evidenced for the first time. This new list is of potential interest for the IASI-NG (Infrared Atmospheric Sounding Interferometer - New Generation) instrument which will be launched on board the METOP-SG satellite in 2025.

## 1. Introduction

The important role played by nitrous acid (HONO) in the chemistry of the troposphere was already mentioned in detail in numerous recent publications [1-3]. Among other infrared absorption bands of this molecule, the 11  $\mu\text{m}$  region is of special atmospheric importance. Its relatively strong signature, with two narrow Q-branches located at 790.117 and 851.943  $\text{cm}^{-1}$  for the *trans*- and *cis*-conformer, respectively, corresponds to a rather clear window of transparency in the Earth atmosphere. Therefore, the 11  $\mu\text{m}$  bands can be used for detection of HONO in the atmosphere by the Infrared Atmospheric Sounding Interferometer (IASI) instrument [4] during exceptional conditions of the large wildfires. This was the case during the large Australian bush fires of February 2009 [5, 6] or in 2019/2020 [7, 8] and more recently, for the detection of HONO enhancements within concentrated fire plumes worldwide [9]. The three IASI instruments are thermal infrared nadir<sup>1</sup> Fourier Transform Spectrometers (operating in the 3.5 - 15.5  $\mu\text{m}$  spectral range), which are implemented on the series of METOP satellites. Very soon, the IASI instruments will be followed by the Infrared Atmospheric Sounding Interferometer New Generation (IASI-NG; <https://iasi-ng.cnes.fr/fr>). IASI-NG is a key payload element of the second generation of European meteorological polar-orbit satellites (METOP-SG) dedicated to operational atmospheric nadir soundings. For IASI-NG, the performance objective is mainly a spectral resolution and a radiometric error improved by a factor of two compared to the IASI first generation ones. One can presume that the possible quantification of trace species from space like HONO will be easier with IASI-NG than with IASI. It is important to prepare and optimize such detection in order to take full advantage of the future capacities of IASI-NG.

Until recently, no line-by-line spectroscopic parameters were available for HONO in the common access databases [10, 11]. Such a situation mainly resulted from the difficulty of measuring line intensities for HONO as it required knowledge of the partial pressures of *trans*-HONO and *cis*-HONO in the cell during the recording of the laboratory spectra. These partial pressures are not easily available because HONO only exists in equilibrium mixtures involving several species and it involves two conformers (*trans*- and *cis*-HONO).

---

<sup>1</sup> Nadir is the downward-facing viewing geometry of an orbiting satellite during remote sensing of the atmosphere.

Accordingly, for their first HONO detection in IASI spectra, Clarisse *et al.* [5], De Longueville *et al.* [7], and Franco *et al.* [9] relied on the HONO infrared absorption cross sections available in the Pacific Northwest National Laboratory (PNNL) database [12]. As they were only available at 296 K, the temperature dependence of the 11  $\mu\text{m}$  signatures was however not accounted for. Indeed, at low temperatures, the *cis*-HONO signature at 851.943  $\text{cm}^{-1}$  tends to decrease notably in favor of that of *trans*-HONO located at 790.117  $\text{cm}^{-1}$ . This behavior results from the fact that the ground state energy levels of the *cis* conformer are located about  $\Delta E_{\text{cis-trans}} \approx 100 \text{ cm}^{-1}$  above those of the *trans* conformer.

To try and compensate for such a dearth of line-by-line spectroscopic information, we generated in 2019 [6] a line list (individual line positions and intensities) for the  $\nu_4$  bands of HONO. This line list [6], hereafter identified as the ‘‘Old’’ line list, has also been used during the recent analysis of the 2019/2020 wildfires in Australia by IASI instruments [8]. For the generation of this line list, we used the line positions and intensities available at that time in the literature. The positions were generated using the vibrational energies and rotational constants for the ground states [13] and the  $4^1$  excited states [14] of *trans*-HONO et *cis*-HONO. More explicitly, for the upper  $4^1$  state, the rotational constants were marginally readjusted from those of Kleiner *et al.* [14] using the following expression:

$$\text{New } X_4 = (\text{Kleiner } X_4 - \text{Kleiner } X_0) + \text{Dehayem } X_0 \quad \text{Eq. (1)}$$

In this expression,  $\text{Kleiner } X_0$  and  $\text{Kleiner } X_4$  are the rotational or centrifugal constants for the ground and  $4^1$  excited stated quoted in Ref. [14], while  $\text{Dehayem } X_0$  is the corresponding ground state value in Ref. [13]. For the computation of lower state energies of *cis*-HONO, and for the intensities of both conformers, it was necessary to choose a value for the energy difference  $\Delta E_{\text{cis-trans}}$  between the *cis* and *trans*  $J = 0$  energy levels. As explained in Ref. [15], several values for this energy difference exist in the literature

For the line list generated in 2019, we used the (rather arbitrary) value  $^{\text{KM}}\Delta E_{\text{cis-trans}} \approx 143 \text{ cm}^{-1}$  which is the one adopted by Kagann and Maki [16]. This is because our 2019 line intensities were scaled in absolute relative to the cross sections quoted in the PNNL database. In fact, these PNNL cross sections are also calibrated in absolute, relative to the band intensity measurements performed by Kagann and Maki [16].

The *trans*-HONO and *cis*-HONO conformers are  $C_s$ -type molecules. For symmetry reasons, both A-type and B-type transitions are presumed to be observable for both  $\nu_4$  bands of

the two conformers. In fact, because the orientations of the molecular dipole moments notably differ, the  $\nu_4$  band of *cis*-HONO is hybrid (both A and B type components), while only A-type transitions are observed for *trans*-HONO. For the 2019 list, we used the information provided in Ref. [14] to estimate the relative contributions of the A-type to B-type character of the  $\nu_4$  band of *cis*-HONO. In addition, we used the PNNL cross sections to determine the absolute intensities of the  $\nu_4$  bands of the *trans*- and *cis*-HONO. This was an uneasy and inaccurate estimation, considering that both conformers contribute to the intensities in the overall frequency range of the 11  $\mu\text{m}$  region. This is particularly the case for the 790.117 to 851.943  $\text{cm}^{-1}$  region, located between the positions of the *trans*- and *cis*- Q branch structures.

For the generation of the presented improved line list, we could benefit from several new experimental data:

✕ A careful investigation of the far-infrared spectral region of HONO was performed relying on Fourier transform spectra recorded at three temperatures on the AILES beamline of the synchrotron SOLEIL. Comparisons of relative line intensities for a large set of B-type transitions for *trans*- and *cis*-HONO led to the significant improvement of the accuracy of the *cis-trans* energy difference  $\Delta E_{\text{cis-trans}} = 95.8 \pm 9.2 \text{ cm}^{-1}$  as compared to the previous infrared determination achieved by Sironneau et al. <sup>Sironneau</sup>  $\Delta E_{\text{cis-trans}} = 99 \pm 25 \text{ cm}^{-1}$  for HONO [17]. Finally, one has also to mention that our value is very close with the recent *ab initio* predictions of Richter et al. [18], that stated <sup>Ab-Initio</sup>  $\Delta E_{\text{cis-trans}} = 93 \text{ cm}^{-1}$ .

In addition, absolute line intensities were generated for the pure rotational bands of *trans*-HONO and *cis*-HONO in the THz to far-infrared region, relying on the well-known *trans*-HONO and *cis*-HONO permanent dipole moments, thanks to Stark measurements [19].

✕ A novel, dual-beam THz/mid-IR experimental setup was developed at the LISA facility in Créteil, France designated as the QUASARS (QUAntitative Spectroscopy for Atmospheric Remote Sensing) set-up [20]. This set-up enables the absolute calibration of the line intensities in the 11  $\mu\text{m}$  region relative to the THz region: the partial pressure of HONO in the sample mixture is determined from the ratio of measured intensities of pure rotation lines to their available absolute line intensities [15], and then used to determine absolute line intensities at 11  $\mu\text{m}$ .

✕ A large set of Fourier transform spectra were recorded at 11  $\mu\text{m}$  using the dual-beam THz/mid-IR QUASARS experimental setup. A large number of absolute line intensities were measured for the  $\nu_4$  bands of *trans*-HONO and *cis*-HONO. These experimental data were also

used to determine the parameters involved in the expansion of the  $\nu_4$  transition operators of the *trans*-HONO and *cis*-HONO and to improve the quality of the existing line positions for these two bands [14].

The present paper is organised in the following way. First, details are provided on the experimental spectra recorded during the present study. Then, the line position investigation for the  $\nu_4$  bands of *trans*-HONO and *cis*-HONO is described, followed by the absolute line intensity measurements that led to the generation of transition moment operators for the  $\nu_4$  bands of both conformers. The last part of the article describes the generation of the final line list, followed by comparisons of computed absorption cross sections with those available in the PNNL database [12]. Spectra calculated using the line list generated in the present work and the “Old” one are compared with some of the high-resolution spectra recorded.

## 2. Experimental details

Absorption spectra of nitrous acid have been recorded using the Fourier transform spectrometer (FTS) and a scanning THz spectrometer, coupled and operating simultaneously on the same sample in the same absorption cross cell made of inert materials, in the QUASARS project located at the LISA facility in Créteil (France). As this setup is fully described elsewhere [20], only a few relevant details are given here. The setup involves a newly constructed temperature-controlled (200-350 K) cross-shaped absorption cell made of inert materials. The cell is traversed by the mid-IR beam from a high-resolution Fourier transform spectrometer along a White-type optics providing absorption path lengths from 2.8 to 42 m and by a single pass (40 cm) of a THz radiation beam (82.5 GHz to 1.1 THz range). The two absorption channels therefore probe simultaneously the same gaseous sample at the same temperature and total pressure. The THz channel can record pure rotational lines of the chemically unstable HONO molecule, for which the (absolute) line intensities were previously determined [15]. This allows a precise determination of the partial pressure in the gaseous mixture, and therefore an absolute calibration for the line intensities at 11  $\mu\text{m}$ .

The IR measurement channel was used to record spectra of HONO in the 11  $\mu\text{m}$  region. The FTS was equipped with a silicon carbide Globar source, a KBr/Ge beamsplitter and an optimized home-made MCT detector [21], using cold aperture, focusing optics and bandpass optical filter of 650-960  $\text{cm}^{-1}$  to improve the signal-to-noise ratio (S/N). The FTS was continuously evacuated below 7 Pa by a dry pump to minimize absorption by atmospheric gases. The diameter of the entrance aperture of the spectrometer was set to 1.7 mm, to maximize

the intensity of IR radiation falling onto the detector without saturation or loss of spectral resolution. Interferograms were recorded with a 80 kHz scanner frequency and a maximum optical path difference (MOPD) of 428.57 cm. According to the Bruker definition (resolution =  $0.9 / \text{MOPD}$ ), this corresponds to a resolution of  $0.0021 \text{ cm}^{-1}$ . The spectra were obtained by Fourier transformation of the interferograms using a Mertz-phase correction,  $1 \text{ cm}^{-1}$  phase resolution, a zero-filling factor of 2 and no apodization (boxcar option).

As HONO is adsorbed and reacts on metal or oxidizable surfaces [22], the cell body and all surfaces in contact with the gas to be measured are constructed of glass, polytetrafluoroethylene (PTFE) or PTFE-coated metal parts. The optical windows are made of silica for the viewports, diamond for the IR windows and PTFE for the THz windows. For the present work, the IR optical path length was set to 5.52 (2) m and all the spectra were recorded at room temperature ( $294 \pm 1 \text{ K}$ ). The inner cell and gas manifold are evacuated with a turbo pump down to  $3 \times 10^{-6} \text{ hPa}$  and the cell pressure is measured either with a 1.1 or 11 hPa range capacitive gauge with ceramic membrane (Pfeiffer, Asslar, Germany), with a reading accuracy of 0.15% according to the manufacturer's specification.

The following procedure was used for the measurements. A background spectrum was first recorded at a resolution of  $0.02 \text{ cm}^{-1}$  while the cell was being continuously evacuated. Then, HONO was directly synthesized in the absorption cross cell by mixing measured amounts of NO, NO<sub>2</sub>, and gaseous H<sub>2</sub>O, thus following the procedure of Ref. [16]. NO<sub>2</sub>, H<sub>2</sub>O and NO were successively introduced into the cell with a mixture composition involving on average 23.76% NO<sub>2</sub>, 31.56% H<sub>2</sub>O and 44.68% NO. The reaction evolved spontaneously towards the formation of HONO and, after about 1h, the equilibrium was reached and the reaction stopped evolving, reaching proportions of 0.3–0.7% of HONO. Spectra were recorded for six different HONO equilibrium mixtures. The six pressures chosen and the number of interferograms recorded and averaged to yield the corresponding spectra are listed in **Table 1**. All the sample spectra were ratioed against the empty cell background spectrum. The root mean square (RMS) S/N in the ratioed spectra ranged between 250 and 500.

The spectra were calibrated by matching the measured positions of 30 lines of residual CO<sub>2</sub> and HNO<sub>3</sub> observed therein to reference wavenumbers available in HITRAN [10] with a root mean square (RMS) deviation of  $0.00011 \text{ cm}^{-1}$ . The absolute accuracy of the measured HONO line positions was estimated as the square root of the sum of squares of the accuracy of the reference CO<sub>2</sub> and HNO<sub>3</sub> line positions in HITRAN (better than  $0.0001 \text{ cm}^{-1}$ ) plus twice the RMS deviation between the observed frequencies and values listed in HITRAN for CO<sub>2</sub> and

HNO<sub>3</sub>, yielding in total 0.00024 cm<sup>-1</sup>. Figure 1 provides an overview of the HONO spectra recorded in this work. The distinctive shape of the A-type  $\nu_4$  bands of *trans*-HONO and *cis*-HONO with their narrow Q-branches are clearly visible.

Simultaneously, on the same samples, we recorded the THz spectra of a few pure rotational lines of nitrous acid to determine the partial pressure of HONO in the mixture. The THz measurement channel uses a monochromatic THz source coupled to the measurement cross cell, presently in a single pass configuration, orientated orthogonally to the IR measurement beam. The source is an amplified multiplier chain (Virginia Diodes, SGX) that can operate at frequencies from 82.5 to 1100 GHz, and is able to produce power levels from 0.1 W to 25  $\mu$ W depending on the installed multiplier stages. For the present work, the stage covering 250-375 GHz was selected as a good compromise between the available source power and HONO molecular line strength. The divergent beam is collimated by a 50 mm focal length TPX lens and propagated through the measurement cell. A second identical TPX lens is used to focus the beam onto a Quasi-Optical Detector (QOD). The QOD is sensitive to frequencies from 100 GHz to 1 THz, and has a responsivity of 200 V/W in the band used in this study. In order to isolate the molecular signal, the source is modulated directly by the microwave synthesizer. Two different modulation schemes [amplitude modulation (AM) and frequency modulation (FM)] can be employed, both of which use a lock-in amplifier to extract the measurement from the detected signal. In the present work, we have used frequency modulation and as a result the signal measured by the lock-in at the frequency of the applied modulation is close to the first derivative of the absorption profile [23]. The signal is obtained at twice the modulation frequency (2F) giving a profile close to the second derivative. Greater sensitivity is achieved because baseline effects are strongly suppressed. The instrument is controlled by a dedicated computer program to instruct the synthesizer frequency, and record the detected signal. A small frequency step is applied to build a complete spectrum point by point. In total, we recorded the THz spectra of 6 pure rotational lines of nitrous acid centred at 297.061, 310.010, 329.926, 340.447, 342.202 and 361.821 GHz. As an example, Figure 2 presents a pure rotational line of *cis*-HONO recorded at different total pressures of the mixtures with a modulation depth of 1080 kHz and a 2F modulation frequency with  $F = 17.013$  kHz. A broadening of the lines is observed, limiting the measurements to a total pressure of 2 hPa.

### 3. Line positions

We used the Fourier transform spectra recorded during this work to perform a new extended investigation of the  $\nu_4$  bands of *trans*-HONO and *cis*-HONO.

During this analysis, the energy levels of the ground states of *trans*-HONO and *cis*-HONO were computed using a Watson's A-type Hamiltonian written in the  $I'$  representation. For the energy levels of the  $4^1$  excited states, this was also the case for *trans*-HONO as well as during the preliminary step of the computation for *cis*-HONO.

As far as the ground states of these species are concerned, we used, without modification, the rotational and centrifugal distortion constants<sup>2</sup> reported by Dehayem *et al.* [13] for the ground vibrational states of *trans*-HONO and *cis*-HONO. The first line positions assignments for the  $\nu_4$  bands were performed using the predictions provided in our "Old" line list, that is based, for the upper states rotational parameters, on the results achieved in Ref. [14] for the  $\nu_4$  bands. Let us remind that this "Old" line list involves both A- and B-type transitions for *cis*-HONO and only A-type transitions for *trans*-HONO. Indeed, as in Ref. [14], searching for B-type transitions for the  $\nu_4$  band of *trans*-HONO proved to be unsuccessful.

It appeared quickly that the observed line positions differ from the 2019's prediction. Therefore, it was clear that the vibrational and rotational parameters of the  $4^1$  states needed to be updated, and this was done iteratively through series of least squares computation performed on the experimental energy levels.

For both conformers, the set of  $4^1$  observed upper state energy levels were obtained by adding the first observed line positions to the calculated ground state levels and introduced in a least squares fit calculation in order to get an improved set of  $4^1$  rotational parameters, and therefore an improved prediction for the  $\nu_4$  line positions, and therefore new assignments. By successive iterations, the analysis could be pursued to its end without difficulties for *trans*-HONO, but was slightly more complicated for *cis*-HONO. Indeed, to correctly predict the line positions for the transitions involving high  $K_a$  values of *cis*-HONO, we had to account for an unexpected B- type Coriolis resonance that couples together the  $4^1$  and  $6^1$  rotational energy levels.

---

<sup>2</sup> As mentioned in Ref. [16], we noted a typing error in Table 2 of Ref. [12] for *cis*-HONO, and we used  $H_{KJ} = -0.678 \times 10^{-9} \text{ cm}^{-1}$ , instead of  $H_{KJ} = -0.0678 \times 10^{-9} \text{ cm}^{-1}$ .

The global results of this analysis, in term of upper J and  $K_a$  values in the  $4^1$  upper states of *trans*-HONO and *cis*-HONO are described shortly in **Table 2**. One can note an improvement in term of the J and  $K_a$  rotational quantum numbers coverage, as compared to the previous investigation performed in Ref. [14], since at that time the analysis was performed up to  $J=50$  and  $K_a=16$ .

For *trans*-HONO, the  $4^1$  energy levels were computed using a simple Watson type rotational Hamiltonian. However, for the *cis*-HONO conformer, we noticed that the energy levels computation was not fully satisfactory. More explicitly, significant discrepancies, up to  $0.009\text{ cm}^{-1}$ , were observed for the series of energy levels of the  $4^1$  state that involve, as rotational quantum numbers,  $K_a=14$  and rather high J values ( $31 \leq J \leq 36$ ). It appeared that this is due to a local ( $\Delta K_a=3$ ) B type Coriolis resonance that couples together the  $K_a=14$  energy levels of the  $4^1$  state together with those in  $K_a=17$  of the  $6^1$  state. In Ref. [24], we investigated the  $\nu_6$  band of *cis*-HONO, and at this occasion, the strong A- and B-type Coriolis interactions linking together the energy levels from the  $6^1$  vibrational state with those from the  $5^1$  one were accounted for. For these reasons, the present final  $4^1$  energy levels computation involves three interacting states  $\{5^1, 6^1, 4^1\}$ , and the form of the Hamiltonian matrix is given in Table 3. In the least squares fit computation we introduced the  $4^1$  energy levels together with those belonging to the  $6^1$  state that were observed during our previous investigation of the  $\nu_6$  band of *cis*-HONO [24]. Let us remind that at this occasion the identification of the very weak  $\nu_5$  band was impossible for *cis*-HONO.

The set of position parameters (vibrational energy, rotational constants, centrifugal distortion constants) that were obtained during this least squared fit for the  $4^1$  vibrational states of *trans*-HONO and *cis*-HONO are gathered, together with their associated uncertainties, in **Tables 4** and **5**, respectively. These Tables provide also the comparison with the values obtained previously for the same constants in Ref. [14].

The results of our energy level computation are quite satisfactory for *trans*-HONO since 96.3% of the 785 levels were reproduced within  $1 \times 10^{-3}\text{ cm}^{-1}$  and also satisfactory for *cis*-HONO. Indeed, 99.2 % of the (825) levels of the  $4^1$  levels and 86.4 % of the (661) of the  $6^1$  energy levels were reproduced with the  $1 \times 10^{-3}\text{ cm}^{-1}$  limit. The root mean square is of  $0.288 \times 10^{-3}\text{ cm}^{-1}$  and  $0.235 \times 10^{-3}\text{ cm}^{-1}$  for the *trans*-HONO and *cis*-HONO computation, respectively.

Accounting for this additional  $4^1 \leftrightarrow 6^1$  ( $\Delta K_a = 3$ ) B-type Coriolis resonance does not change significantly the quality of the computation for the  $6^1$  energy levels, nor the values of the parameters describing the  $5^1 \leftrightarrow 6^1$  interacting states, as compared to the results of Ref. [24].

On the contrary, considering this resonance increases the quality of the computation for the  $4^1$  levels. Indeed, for the series of levels involving  $K_a = 14$  the differences between observed and computed energy levels goes down to less than  $0.5 \times 10^{-3} \text{ cm}^{-1}$ , to be compared to the large Obs-Calc up to  $-0.009 \text{ cm}^{-1}$  for  $J = 36$  achieved when this resonance is ignored. In parallel, the percentage of mixing of the  $4^1$  wavefunctions of levels involving  $K_a = 14$  with those from  $6^1$  involving  $K_a = 17$  increases with  $J$ , from 0% for  $J = 30$  up to 2.05 % for  $J = 36$ .

It is necessary to compare, relative to Ref. [14], the quality of the prediction provided by the constants obtained in this work for the  $4^1$  state of *trans*-HONO and for the  $\{5^1, 6^1, 4^1\}$  interacting states for *cis*-HONO.

For this, we made a direct energy level computation using the  $v = 4^1$  vibrational energies and rotational constants that are collected in Table I of Ref. [14] for *trans*-HONO and *cis*-HONO. As expected, the computed line positions for  $v = 4^1$  differ from the observed ones for the high  $K_a$  values. Indeed, our analysis of the  $v_4$  bands was pursued up to higher  $K_a$  values for both conformers than in the previous investigation.

However, for both *trans*-HONO and *cis*-HONO we also noticed significant discrepancies between the observed and computed values for energy levels involving very low  $K_a$  values ( $K_a \leq 1$ ) starting from the medium  $J$  values ( $J \geq 25$ ). To illustrate this point, Fig. 3 presents, for *trans*-HONO and *cis*-HONO, the plotted differences between the computed and observed  $v = 4^1$  energy levels that involve  $K_a = 0$ . When inspecting Tables 4 and 5 it is clear that several centrifugal distortion parameters achieved in this work differ, within their estimated uncertainty, from the values achieved in Ref. [14]. According to several test calculations, we identified the  $\delta_J$  centrifugal distortion parameters for the  $v = 4^1$  states of *trans*-HONO and *cis*-HONO [14] as the responsible for the largest discrepancies.

As a conclusion it is clear that making a new high resolution detailed analysis of these  $v_4$  bands was quite useful for getting more accurate line positions.

## 4. Retrieval of line intensities and uncertainty analysis

### 4.1. Determination of HONO partial pressure for quantification of the 11 $\mu\text{m}$ region

The THz spectra of the 6 pure rotational lines of nitrous acid were analyzed using a program developed for this purpose. As this software will be described in a separate publication, only a very brief description is provided here. The program can calculate or fit amplitude or frequency modulated (2F) THz absorption spectra, dealing with any number of spectral ranges belonging to the same or different spectra. Observed spectra are modeled as the convolution of the molecular transmission spectrum with an instrument line shape (ILS). The ILS is a Gaussian of adjustable width for the amplitude modulated spectra and is modeled according to Dore [25] for the 2F frequency modulated spectra. Figure 4 displays an example of the result of fitting the second harmonic profile of the pure rotational transition of *cis*-HONO shown in Fig. 2. In the adjustment, the line intensity was held fixed to the value calculated using the expansion of the permanent dipole moment [15], while the mixing ratio of the HONO molecule was fitted, as well as the effective broadening coefficient by the buffer gas in the mixture (mainly NO<sub>2</sub>, H<sub>2</sub>O and NO). For a line belonging to the active molecule (HONO), the pressure induced broadening is calculated according to

$$\gamma_L = [b_L^0(\text{self}) x + b_L^0(\text{buffer}) (1 - x)] P_{tot} \quad \text{Eq. (2)}$$

where  $x$  is the mixing ratio of the active molecule,  $P_{tot}$  is the total pressure,  $b_L^0(\text{self})$  is the self-broadening coefficient and  $b_L^0(\text{buffer})$  the effective buffer-gas broadening coefficient. Given the small HONO partial pressure, the self-broadening contribution is very weak in comparison to buffer-broadening contribution, so it was fixed to 3 MHz/hPa. The absence of signatures out of the spectral noise in the residuals presented in Fig. 4 indicates that the Voigt profile is adequate to fit the observed line. The partial pressure of HONO in the gas mixture is determined from the mixing ratio:

$$P_{HONO} = x \times P_{tot} \quad \text{Eq. (3)}$$

From Eq. (3), we deduce the absolute uncertainty on the partial pressure of HONO, according to the formula:

$$\Delta P_{HONO} = \left( \frac{\Delta x}{x} + \frac{\Delta P_{tot}}{P_{tot}} \right) \times P_{HONO} \quad \text{Eq. (4)}$$

$\Delta x$  is given by the standard deviation of the fit and  $\Delta P_{tot}$  is obtained from the accuracy on the total pressure reading. For this experiment series, total nitrous acid partial pressures ranging from 0.00131 to 0.01431 hPa were determined and given with their uncertainty in the third column of **Table 1**. On average, the relative uncertainty on the partial pressure of HONO is equal to 2.3%. These partial pressures are used for absolute IR line intensity determinations, as explained below.

#### 4.2. Retrieval of line intensities in the 11 $\mu\text{m}$ region

The IR line intensities were measured using a multi-spectrum fitting program developed previously in Brussels [26, 27]. This program adjusts spectroscopic (e.g. line positions, intensities and widths) and spectrum-specific (e.g. baseline) parameters to best-fit synthetic spectra to the observed spectra using a Levenberg-Marquardt non-linear least squares fitting procedure. Each synthetic spectrum is calculated as the convolution of the molecular transmission spectrum with an instrument line shape function, which includes the effects of the finite maximum optical path difference and of the finite source aperture diameter of the interferometer. In the present work, no deviation from this model instrument line shape was observed using the nominal aperture diameter of 1.7 mm. The molecular transmission spectrum was generated on a wavenumber grid characterized by a point spacing 4 times smaller than in the corresponding observed spectrum. After convolution with the instrument line shape function, only the calculated spectral points corresponding to observed spectral points were retained. The background in each spectrum was represented by a polynomial expansion up to the second order (a constant or an affine function was however found sufficient in most cases), and the profile of the lines was modeled using a Voigt function [28] with Gaussian width always held fixed to the value calculated for the Doppler broadening. The measurements were carried out on spectrally restricted intervals, ranging from 0.07 to 0.3  $\text{cm}^{-1}$  and containing either a single or several lines. The fitted line parameters were the positions, intensities, and buffer-broadening coefficients. The pressure induced broadening is calculated according to Eq. (2). The self-broadening and self-shift coefficients of all the lines were set to 0.1 and 0.0  $\text{cm}^{-1}\text{atm}^{-1}$ , respectively. The buffer-broadening coefficient of all the lines was initially set to 0.2  $\text{cm}^{-1}\text{atm}^{-1}$ , a slightly higher starting value was chosen after some trial and error cycles, which is justified by the greater dipole moment of the main mixture components. The required initial values of the positions and intensities of *trans*- and *cis*-HONO lines considered in the present work were generated during the present study for the positions, and from our previous investigation [6] for the intensities. The HONO partial pressures were those determined from our THz analysis, and their values were kept constant to fit the line intensities. Intensity measurements were made for six spectra at different HONO equilibrium mixtures (see **Table 1**). **Figure 5** presents an example of the results of a fit for the spectrum S2 recorded at 294 K. It contains three lines observed in the spectral range 803.69 to 803.81  $\text{cm}^{-1}$  and a total of ten fitted parameters. The absence of the molecular signatures in the residuals suggests that the Voigt profile is adequate

to fit the observed lines at this level. Finally, in this work, 452 individual lines for *trans*-HONO and 568 for *cis*-HONO were carefully measured.

### 4.3. Uncertainty analysis

Examination of the fit residuals shows that they are generally less than 2%. However, to estimate the accuracy of the measured intensities also requires considering the uncertainties on the physical parameters, contributions from possible systematic errors [29] as well as the uncertainties derived from the fits, taken as the standard deviation. The various sources of error considered in the present work and their associated uncertainties expressed relative to the line intensities are given in **Fig. 6** for three strong, medium and weak selected lines, representative of the 1020 measured lines, i.e. <sup>Q</sup>R (17,1), <sup>Q</sup>R (14,10) and <sup>Q</sup>P (16,12). **Figure 6** shows that pressure, systematic errors and the standard deviations of the fits are the main sources of error. The dominant contributions to the systematic errors arise from shifts in the location of the full-scale (100%) photometric level or measurement noise. The effect of noise and small baseline offsets in these were also considered. The 0% level could be checked readily and the 100% level fitted on the spectra in regions without absorptions. In the end, for systematic errors, an arbitrary, but conservative estimate of 2% of the line intensities has been retained here. For each transition, we then calculated an upper limit for the overall uncertainty based on the maximum uncertainty of the individual experimental parameters, i.e.  $\varepsilon_{si}$  (sample purity),  $\varepsilon_t$  (temperature),  $\varepsilon_p$  (pressure),  $\varepsilon_{pl}$  (pathlength),  $\varepsilon_{fit}$  (standard deviation from fit) and  $\varepsilon_{sys}$  (systematic errors), assuming that these uncertainties are uncorrelated:

$$\varepsilon = \sqrt{\varepsilon_{si}^2 + \varepsilon_t^2 + \varepsilon_p^2 + \varepsilon_{pl}^2 + \varepsilon_{fit}^2 + \varepsilon_{sys}^2} \quad \text{Eq. (5)}$$

Using Eq. (5) and the experimental relative uncertainties involved, the estimated overall uncertainty (estimated accuracy) for each of the 1020 line intensities measured was calculated. On average, the estimated accuracy for line intensities is equal to 5 %.

## 5. Line intensity calculations

The method used to compute line intensities for HONO was already described in detail in Ref. [15]. However, the equation used to describe the line intensity of a given line of

$\text{H}^{16}\text{O}^{14}\text{N}^{16}\text{O}$  in a “natural sample” of nitrous acid (in  $\text{cm}^{-1}/(\text{molecule} \cdot \text{cm}^{-2})$ ) differs slightly, for *trans*-HONO and *cis*-HONO. For the *trans*-HONO conformer form, this intensity is given as:

$${}^{trans}k_{\tilde{\nu}}^N(T) = a_{iso} \frac{8\pi^3\tilde{\nu}}{4\pi\epsilon_0 3hc^{\text{TotZ}}(T)} g_{nucl} \left(1 - \exp\left(-\frac{hc\tilde{\nu}}{kT}\right)\right) \exp\left(-\frac{hcE_A}{kT}\right) R_A^B \quad \text{Eq. (6)}$$

while, for the *cis*-conformer form, we used a slightly different expression:

$$\begin{aligned} {}^{cis}k_{\tilde{\nu}}^N(T) &= \exp\left(-\frac{hc\Delta E_{cis-trans}}{kT}\right) \times \\ &\dots a_{iso} \frac{8\pi^3\tilde{\nu}}{4\pi\epsilon_0 3hc^{\text{TotZ}}(T)} g_{nucl} \left(1 - \exp\left(-\frac{hc\tilde{\nu}}{kT}\right)\right) \exp\left(-\frac{hcE_A}{kT}\right) R_A^B \end{aligned} \quad \text{Eq.(7)}$$

Indeed, for the *cis*-conformer, Eq. (7) includes the “ $\exp\left(-\frac{hc\Delta E_{cis-trans}}{kT}\right)$ ” term to account for the definition of the  $J = 0$  level of the *cis*-conformer relative to the *trans*-one. In these expressions, the letters “A” and “B” and  ${}^{trans}E_A(J, K_a, K_c)$  and  ${}^{trans}E_B(J, K_a, K_c)$  (respectively,  ${}^{cis}E_A(J, K_a, K_c)$  and  ${}^{cis}E_B(J, K_a, K_c)$ ) are the upper and lower computed wavefunctions and energies of the levels relatively to the  $J = 0$  energy level for *trans*-HONO (respectively, for *cis*-HONO) using the parameters quoted in Tables 1 and 2 of Ref. [13] for *trans*-HONO and *cis*-HONO, respectively. Indeed, accordingly, the definition of the lower level and upper level of the transition,  $E_L$  and  $E_U$  respectively, differ for *trans*-HONO and *cis*-HONO, since one has:

$${}^{trans}E_L = {}^{trans}E_A(J, K_a, K_c) \text{ and } {}^{trans}E_U = {}^{trans}E_B(J, K_a, K_c) \quad \text{Eq. (8)}$$

and

$${}^{cis}E_L = {}^{cis}E_A(J, K_a, K_c) + \Delta E_{cis-trans} \text{ and } {}^{cis}E_U = {}^{cis}E_B(J, K_a, K_c) + \Delta E_{cis-trans} \quad \text{Eq. (9)}$$

In addition,

- $\tilde{\nu}$  is the wavenumber in  $\text{cm}^{-1}$ , and one has:

$$\tilde{\nu} = (E_B - E_A) = (E_L - E_U) \quad \text{Eq. (10)}$$

- $a_{iso} = 0.9937$  is the isotopic abundance of  $\text{H}^{16}\text{O}^{14}\text{N}^{16}\text{O}$  in a “natural sample” of nitrous acid.
- $g_{nucl}$  is the nuclear spin factor, which is set to a constant value ( $g_{nucl} = 1$ ) for all rotational levels of the *cis*- and *trans*-HONO, will be omitted in the rest of the discussion. This is because we do not consider here the hyperfine structure due to the non-zero nuclear spin for hydrogen and nitrogen.

- ${}^{\text{Tot}}Z(T)$  is the “total” partition function of HONO at the temperature  $T$ , which includes a contribution from the *trans*- and *cis*-conformers,  ${}^{\text{trans}}Z(T)$  and  ${}^{\text{cis}}Z(T)$ , respectively.

$${}^{\text{Tot}}Z(T) = {}^{\text{trans}}Z(T) + {}^{\text{cis}}Z(T) \times {}^{\text{cis-trans}}Z(T) \quad \text{Eq. (11)}$$

In this latter expression, the term

$${}^{\text{cis-trans}}Z(T) = \exp\left(-\frac{hc\Delta E_{\text{cis-trans}}}{kT}\right) \quad \text{Eq. (12)}$$

accounts for the population ratio of the rotational levels of *cis*-HONO relative to those of *trans*-HONO, because of the convention adopted for the  $J = 0$  level of *cis*-HONO. This term was computed using the value  $\Delta E_{\text{cis-trans}} = 95.8 \pm 9.2 \text{ cm}^{-1}$  [15].

In addition,  ${}^{\text{trans}}Z(T)$  and  ${}^{\text{cis}}Z(T)$  in Eq. (11) are the “classical” vibration-rotation contributions of *trans*-HONO and *cis*-HONO that are computed as usual [30] in the Harmonic Oscillator Approximation (HOA) as the product of its vibrational and rotational contributions, i.e. for the *trans*-form and *cis*-form, as:

$${}^{\text{trans}}Z(T) = {}^{\text{trans}}Z_{\text{Vib}}(T) \times {}^{\text{trans}}Z_{\text{Rot}}(T)$$

and

$${}^{\text{cis}}Z(T) = {}^{\text{cis}}Z_{\text{Vib}}(T) \times {}^{\text{cis}}Z_{\text{Rot}}(T) \quad \text{Eqs. (13)}$$

More details on the computation of the  ${}^{\text{Tot}}Z(T)$  are provided in Ref. [15]. In the present work, we used the numerical values  ${}^{\text{Tot}}Z(296\text{K}) = 14302.75$  and  ${}^{\text{Tot}}Z(294\text{K}) = 14098.99$  quoted as Supplementary data of that paper.

- In Eq. (6) (resp. Eq. (7)), the *trans*- (resp. *cis*-)  $R_A^B$  factors, are the square of the matrix element of the  $\nu_4$  transformed transition moment operator  $\mu_Z'$  for the *trans*-conformer (resp. *cis*-conformer). For the *trans*-conformer form, one can write:

$$R_L^U = \left| \langle 4, J' K_a' K_c' | {}^{\text{trans}}\mu_Z' | 0, J'' K_a'' K_c'' \rangle \right|^2, \quad \text{Eq. (14)}$$

where  $|4\rangle$  and  $|0\rangle$  are the upper and lower vibrational states of the transition, and  ${}^{\text{trans}}\mu_Z'$  is the Z-component of the transformed transition moment operator for the *trans*-conformer form [31]. A similar expression can be written for *cis*-HONO.

Both the *trans*-HONO and *cis*-HONO are planar  $C_s$ -type molecules, and following symmetry considerations, both A- and B-type rotational transitions are to be observed for the far infrared bands with  $(\Delta K_a = 0, \Delta K_c = \pm 1)$  and  $(\Delta K_a = \pm 1, \Delta K_c = \pm 1)$  selection rules, respectively, on the  $K_a$  and  $K_c$  rotational quantum numbers. In fact, the search of B-type transitions for the  $\nu_4$  band of *trans*-HONO proved to be unsuccessful. The method used to expand the  $\nu_4$  transformed transition moment operators is described in detail in Ref. [31]. The terms that proved to be of significant contribution to the observed intensities are given in the next two equations:

$${}^{trans}\mu' = {}^{trans}\mu_1^A \times \varphi_z + {}^{trans}\mu_4^A \times 1/2(\{\varphi_x, iJ_y\} - \{i\varphi_y, J_x\}) \quad \text{Eq. (15)}$$

$${}^{cis}\mu' = {}^{cis}\mu_1^B \times \varphi_x + {}^{cis}\mu_1^A \times \varphi_z + {}^{cis}\mu_4^A \times 1/2(\{\varphi_x, iJ_y\} - \{i\varphi_y, J_x\}) \quad \text{Eq. (16)}$$

The experimental line intensities measured during this work for the  $\nu_4$  bands of *trans*-HONO and *cis*-HONO were introduced in two least squares calculations. The values obtained for the parameters appearing in the Eqs. (15) and (16) are quoted in **Table 6**. The statistical analysis of the results of these computations is provided in **Table 7**.

## 6. The new line list for the $\nu_4$ bands of *trans*-HONO and *cis*-HONO conformers

- (a) Generation of the list of line positions, line intensities, and line shape parameters for the  $\nu_4$  bands of *trans*-HONO and *cis*-HONO conformers

The method used to generate the complete line list of the  $\nu_4$  bands of HONO was already described in Ref. [6, 14]. The upper and lower state energy levels were computed using the constants that are collected in **Tables 4** and **5** for *trans*-HONO and *cis*-HONO, respectively. The line intensities were computed at 296 K for a minimum limit of  $5 \times 10^{-25} \text{ cm}^{-1}/(\text{molecule} \cdot \text{cm}^{-2})$ , and we used the dipole moment operators that are described in **Table 6**. It is important to remind at that point that we used the more recent and precise  $\Delta E_{\text{cis-trans}} = 95.8 \pm 9.2 \text{ cm}^{-1}$  value [15], instead of  $\Delta E_{\text{cis-trans}} = 147 \text{ cm}^{-1}$  in Ref. [6].

This line list, generated in the HITRAN format [10], also includes line shape parameters. There exists, to our knowledge, no experimental or theoretical estimation of these data in the literature. It appears that the permanent dipole moments of *trans*-HONO and *cis*-HONO have values,  ${}^{\text{Trans}}\mu_0 = 1.930 \text{ D}$  and  ${}^{\text{Cis}}\mu_0 = 1.428 \text{ D}$ , respectively [19], that are close to the water permanent dipole value ( $\mu_0 = 1.855 \text{ D}$  [32]). Therefore, as it was done in Ref. [6], the ‘‘a priori’’ values:

$$\gamma_{\text{Air}} = 0.1 \text{ cm}^{-1}/\text{atm}, \gamma_{\text{Self}} = 0.4 \text{ cm}^{-1}/\text{atm}, \text{ and } n_{\text{Air}} = 0.7 \quad \text{Eq. (17)}$$

that are similar to those of water, were implemented for the air-broadened half-width, self-broadened half-width and the temperature dependence exponent of the air broadening, respectively.

**Table 8** provides a brief description of the line list, in terms of number of lines, frequency range, band intensities and maximum intensities, discriminating for *cis*-HONO the contribution of the A-type and B-type components. Please note that, because of the existence of vibrational rotational resonances coupling together the  $\{4^1, 5^1, 6^1\}$  vibrational states for *cis*-HONO, several (very weak)  $\Delta K_a = 2$  or  $\Delta K_a = 3$  forbidden transitions of the  $\nu_5$  and  $\nu_6$  bands are predicted by our calculation in the 11  $\mu\text{m}$  region for *cis*-HONO. Note that *cis*-HONO possess at 15.6  $\mu\text{m}$  an infrared signature that is similar in strength to the 11  $\mu\text{m}$  one, and corresponds to the  $\nu_6$  band centered at  $639.7432 \text{ cm}^{-1}$  [24]. Future studies should focus in more details than in Ref. [24] the line intensities 15.6  $\mu\text{m}$  region.

#### b) Estimation of the uncertainties on the computed line positions and intensities

Considering that the energy level computation was quite satisfactory, we estimate that the line positions for both conformers are predicted within an accuracy that is better than  $\sim 0.001 \text{ cm}^{-1}$  for lines involving  $J \leq 45$ ,  $K_a \leq 15$ . Indeed, these lines correspond, more or less, to the range of energy levels that were covered by our analysis. As usual, the accuracy is only about  $\approx 0.003 \text{ cm}^{-1}$ , for transitions involving higher rotational quantum numbers.

For the line list, that is generated at 296 K, we estimate the relative uncertainties on the line intensities at 7 % (resp. 9 %) for  $\nu_4$  transitions of *trans*-HONO (resp. *cis*-HONO) conformer involving low to medium J and  $K_a$  values ( $J \leq 30$ ,  $K_a \leq 10$ ), and at 9 % (resp. 15 %) for transitions involving higher values of the rotational quantum numbers. These estimations are based on the estimated accuracy associated with the experimental line intensities and on the quality of the model. Indeed, for *cis*-HONO, the intensity calculation is more complicated than for *trans*-HONO, considering the existence of A-type and both B- type component for *cis*-HONO.

#### c) Impact of the uncertainty associated to $\Delta E_{\text{cis-trans}}$ for the computed line intensities

One has also to evaluate the impact, for the intensities, that is linked to the uncertainty associated to the *cis*- to *trans*-HONO energy difference ( $\Delta E_{\text{cis-trans}} = 95.8 \pm 9.2 \text{ cm}^{-1}$  [15]). A modification of the  $\Delta E_{\text{cis-trans}}$  value induces a change for the lower state energies for the *cis*-HONO lines (see Eq.(9)) and of the computed total partition function  $^{\text{Tot}}Z(T)$  values at a given T temperature. These entities contribute to the intensity calculations, the least squares fit performed, in such conditions, on the experimental line intensities (see paragraph 5) leads to numeral values, for the  $\mu_1^B$  intensity parameters, that differ from those presented in Table 6. These  $\mu_1^B$  values are adjusted to compensate, for the recalculated intensities, the changes induced by  $\Delta E_{\text{cis-trans}}$ . In our case, the experimental intensities used for our fit were established at a temperature value (T=294 K), and the impact on the final intensities, established at T=296 K is of course marginal.

On the contrary, the uncertainty affecting  $\Delta E_{\text{cis-trans}}$  affects somehow the temperature dependence of the line intensities. This is illustrated in Table 9 where we compute the  $\nu_4$  band of *trans*-HONO and *cis*-HONO for a test temperature of T=230 K and for different values of  $\Delta E_{\text{cis-trans}}$ .

At 230K, using  $\Delta E_{\text{cis-trans}} = 86.6 \text{ cm}^{-1}$  (resp.  $\Delta E_{\text{cis-trans}} = 105 \text{ cm}^{-1}$ ) instead of  $\Delta E_{\text{cis-trans}} = 95.8 \text{ cm}^{-1}$  affects mainly the *cis*-HONO line intensities that increased for about +1% (resp. decrease for about -1%).

Also, we note, also that, for  $\Delta E_{\text{cis-trans}} = 95.8 \text{ cm}^{-1}$ , the intensity ratio  $R(T) = \frac{\text{Int}(\text{cis-HONO}, T)}{\text{Int}(\text{trans-HONO}, T)}$

between the *cis*-HONO and *trans*-HONO  $\nu_4$  band intensities at a given T temperature goes down from  $R(296\text{K}) = 1.1295$  to  $R(230\text{K}) = 0.9855$ , proving that the temperature dependence of the intensities is not negligible.

## 7. Comparison with the line list generated in Ref. [6]:

### (a) Band intensities and the PNNL cross sections:

The previous line intensity calculation [6], hereafter defined as the “Old” line list, was performed by scaling in absolute the line intensities relative to the PNNL cross sections [12, 16], which corresponds to the integrated band intensity  $^{\text{PNNL}}S(11 \mu\text{m}, 296 \text{ K}) = 2.862 \times 10^{-17} \text{ cm}^{-1}$

$^{1}/(\text{molecule.cm}^{-2}$  at 296 K in the 720-920  $\text{cm}^{-1}$  spectral region. This value includes contributions from the cold  $\nu_4$  bands of *trans*-HONO and *cis*-HONO, together with those from their associated hot bands. In Ref. [6], we could numerically estimate the relative intensity contribution to  $^{\text{PNNLS}}$  (11  $\mu\text{m}$ , 296 K) that is due to the cold  $\nu_4$  bands of *trans*-HONO and *cis*-HONO using the vibration partition functions,  $^{\text{trans}}Z_{\text{Vib}}(T)$  and  $^{\text{cis}}Z_{\text{Vib}}(T)$ , of *trans*-HONO and *cis*-HONO respectively. These values differ marginally in values at 296 K, and for the whole 11  $\mu\text{m}$  region one can use the value:

$$Z_{\text{Vib}}(296 \text{ K}) \approx 1.16738, \quad \text{Eq. (18)}$$

that is the mean value of  $^{\text{trans}}Z_{\text{Vib}}(T=296 \text{ K})$  and  $^{\text{cis}}Z_{\text{Vib}}(T=296 \text{ K})$ .

Accordingly, one has:

$$(^{\text{Old-trans}}\text{Int}(\nu_4, 296 \text{ K}) + ^{\text{Old-cis}}\text{Int}(\nu_4, 296 \text{ K})) \approx ^{\text{PNNLS}}\text{S}(11 \mu\text{m}, 296 \text{ K}) / Z_{\text{Vib}}(296 \text{ K}) \quad \text{Eq. (19)}$$

In Eq. (19), the  $^{\text{Old-trans}}\text{Int}(\nu_4, 296 \text{ K})$  and  $^{\text{Old-cis}}\text{Int}(\nu_4, 296 \text{ K})$  band intensities are computed, as usual, by summing the individual line intensities of the  $\nu_4$  cold bands. The relative *trans* to *cis* contribution to the intensities at 11  $\mu\text{m}$  was determined by using the PNNL cross sections.

Also, we used the information provided in Ref. [14] to estimate the relative contributions of the A-type to B-type character of the  $\nu_4$  bands. Indeed, the  $\nu_4$  band of *trans*-HONO is an A-type band, while for *cis*-HONO both A- and B-type contributions are to be considered. In this way the following values for the band intensities (in  $\text{cm}^{-1}/(\text{molecule.cm}^{-2})$ ) at 296 K were achieved for the hybrid  $\nu_4$  bands of *trans*- and *cis*-HONO:

$$\begin{aligned} ^{\text{Old-trans}}\text{Int}_{\text{A-type}}(\nu_4, 296 \text{ K}) &= 1.211 \times 10^{-17}, \\ ^{\text{Old-cis}}\text{Int}_{\text{A-type}}(\nu_4, 296 \text{ K}) &= 1.108 \times 10^{-17}, \\ ^{\text{Old-cis}}\text{Int}_{\text{B-type}}(\nu_4, 296 \text{ K}) &= 0.133 \times 10^{-17} \end{aligned} \quad \text{Eqs. (20)}$$

And therefore

$$^{\text{Old}}\text{Int}(\nu_4, 296 \text{ K}) = ^{\text{Old-trans}}\text{Int}(\nu_4, 296 \text{ K}) + ^{\text{Old-cis}}\text{Int}(\nu_4, 296 \text{ K}) = 2.452 \times 10^{-17} \quad \text{Eq. (21)}$$

When comparing these ‘‘Old’’ values [6] with those of **Table 8**, it is clear that, the present calculation leads to intensities that are larger than those estimated in Ref. [6]. More precisely, one has:

$$\text{NewInt}(v_4, 296 \text{ K}) / \text{OldInt}(v_4, 296 \text{ K}) \approx 1.23 \quad \text{Eq. (22)}$$

Therefore, when accounting for the contribution of the hot bands we obtain a computed total integrated band intensity at  $11 \mu\text{m}$   $\text{NewS}(11 \mu\text{m}, 296 \text{ K})$  (see Eqs. 18 and 19, and **Table 8**) that is also  $\sim 23\%$  larger than the PNNL value [12]. Actually, this 23% increase of the band intensities is due to differences between the outputs of our “New” measurements and those of Kagann and Maki [16]. This is because the PNNL absorption cross sections [12] were calibrated in absolute relative to the band intensities obtained by Kagann and Maki [16]. Considering the difficulty to estimate the partial pressure of the various impurities (water, NO, N<sub>2</sub>O, NO<sub>2</sub> etc..) present in the cell together with HONO during laboratory measurements, one may consider this 23 % disagreement as reasonable.

Fig. 7 provides an overview of the comparison of the PNNL absorption cross sections [12] with those computed using the line lists generated in Ref. [6] and in the present work. For an easier comparison, the “old” and “new” individual line intensities were multiplied by a  $Z_{\text{Vib}}(296 \text{ K})$  constant factor (see Eq.(18)), to account, in absolute, for the hot bands contribution. In addition, in the “New” line list, the intensities were also divided by a constant factor of 1.23, and this is because the new intensities are, on the average, about 23 % stronger than those computed previously [6]. One can see that at the resolution of the PNNL cross sections (about  $0.1 \text{ cm}^{-1}$ ) the two computations differ in a rather soft behavior. Clearly, the W-type signatures that are observed in the “Obs-Calc” differences are due to, presumably, the presence of hot bands and/or to the existence in the Q branches of line mixing effects which are not accounted for by either the “Old” [6] or “New” computations.

(b) Comparison with the high-resolution spectrum recorded during this work.

Figure 8 provides an overview of the high-resolution Fourier transform spectrum in the  $740\text{--}900 \text{ cm}^{-1}$  region, together with the line by line models performed using the “Old” [6] and new line lists. The bottom trace in the same figure gives the difference between the two computations, and the largest differences in positions correspond mostly to lines that involve low  $K_a$  ( $K_a = 0, 1$  and  $2$ ) for both conformers. This is because, for the line positions, our “Old” computation was based on the rotational constants of Ref. [14]. Figs. 9 to 13 provide detailed

views in different spectral regions. It is clear that the new computation is of better quality than the previous one.

## 8. Conclusion

In the present work, we performed a new high-resolution investigation of the  $\nu_4$  bands of *trans*-HONO and *cis*-HONO. The line position analyses enabled us to improve the quality of the vibrational energies and rotational constants that exist for the  $4^1$  states of both conformers. Individual line intensities were measured for the  $\nu_4$  bands. These experimental intensities were calibrated in absolute using the method described in Ref. [20] and, then introduced in a least squares fit computation to get the expansion of the transition moment operators of the  $\nu_4$  bands of *trans*-HONO and *cis*-HONO. These improved line position and line intensity parameters were used to generate an improved line list for the  $\nu_4$  bands of *trans*-HONO and *cis*-HONO. In this new line list, the intensities are on the average about 24 % stronger than in our previous version of the same list that was scaled in absolute relative to the PNNL cross sections. This new list is available upon request. Indeed, before diffusing this updated version of 11  $\mu\text{m}$  list for HONO to the whole community, we project to test its quality as compared to its preliminary version [6] through identification of HONO signatures in atmospheric spectra.

## Supplementary data

List of assignments for the  $\nu_4$  bands of *trans*-HONO and *cis*-HONO.

Energy calculation for the  $4^1$  vibrational energy levels of *trans*-HONO and *cis*-HONO.

List of experimental line intensities and computation for the  $\nu_4$  bands of *trans*-HONO and *cis*-HONO.

## ACKNOWLEDGEMENTS

This work was supported by the French National program ANR (ANR-19-CE29-0013) through the « QUASARS » project. The authors want to thank also the AERIS atmospheric and data pole and the CNES French space agency to make available the IASI level 1 data. JVA acknowledges financial support from the ARC program (SPHERES project) of the French Community (Belgium). The LPCA work was supported by the CaPPA project (Chemical and Physical Properties of the Atmosphere) funded by the French National Research Agency (ANR-11-LABX-0005-01) and the ECRIN program supported by the Hauts-de-France Regional

Council, the French Ministry of Higher Education and Research and the European Regional Development Fund.

### References

- [1] Platt U, Perner D, Harris GW, Winer AM, Pitts Jr JN. Observations of nitrous acid in an urban atmosphere by differential optical absorption. *Nature* 1980;285:312–314.
- [2] Yokelson RJ, Crouse JD, DeCarlo PF, Karl T, Urbanski S, Atlas E, Campos T, Shinozuka Y, Kapustin V, Clarke AD, Weinheimer A, Knapp DJ, Montzka DD, Holloway J, Weibring P, Flocke F, Zheng W, Toohey D, Wennberg PO, Wiedinmyer C, Mauldin L, Fried A, Richter D, Walega J, Jimenez JL, Adachi K, Buseck PR, Hall SR, Shetter R. Emissions from biomass burning in the Yucatan. *Atmos Chem Phys* 2009;9:5785–5812.
- [3] Stockwell CE, Yokelson RJ, Kreidenweis SM, Robinson AL, DeMott PJ, Sullivan RC, Reardon J, Ryan KC, Griffith DWT, Stevens L. Trace gas emissions from combustion of peat, crop residue, domestic biofuels, grasses, and other fuels: configuration and Fourier transform infrared (FTIR) component of the fourth Fire Lab at Missoula Experiment (FLAME-4). *Atmos Chem Phys* 2014;14: 9727–9754.
- [4] Clerbaux C, Boynard A, Clarisse L, George M, Hadji-Lazaro J, Herbin H, Hurtmans D, Pommier M, Razavi A, Turquety S, Wespes C, Coheur PF. Monitoring of atmospheric composition using the thermal infrared IASI/MetOp sounder. *Atmos Chem Phys* 2009;9:6041–6054.
- [5] Clarisse L, R'Honi Y, Coheur PF, Hurtmans D, Clerbaux C. Thermal infrared nadir observations of 24 atmospheric gases. *Geophys Res Lett* 2011;38:L10802.
- [6] Armante R, Perrin A, Kwabia Tchana F, Manceron L. The  $\nu_4$  bands at 11  $\mu\text{m}$ : linelists for the *trans*- and *cis*- conformer forms of nitrous acid (HONO) in the 2019 version of the GEISA database. *Mol Phys* 2021;e1951860:1–13.
- [7] De Longueville H, Clarisse L, Whitburn S, Franco B, Bauduin S, Clerbaux C, Camy-Peyret C, Coheur PF. Identification of short and long-lived atmospheric trace gases from IASI space observations. *Geophys Res Lett* 2021;48:L091742.
- [8] Dufour G, Eremenko M, Siour G, Sellitto P, Cuesta J, Perrin A, Beekmann M. 24 h Evolution of an exceptional HONO plume emitted by the record-breaking 2019/2020 Australian wildfire tracked from space. *Atmosphere* 2022;13:1485.
- [9] Franco B, Clarisse L, Theys N, Hadji-Lazaro J, Clerbaux C, and Coheur P. Pyrogenic HONO seen from space: insights from global IASI observations. *Atmos Chem Phys* 2024; 24, 4973–5007.
- [10] Gordon IE, Rothman LS, Hargreaves RJ, Hashemi R, Karlovets EV, Skinner FM, Conway EK, Hill C, Kochanov RV, Tan Y, Wcisłó P, Finenko AA, Nelson K, Bernath PF, Birk M, Boudon V, Campargue A, Chance KV, Coustenis A, Drouin BJ, Flaud J-M,

- Gamache RR, Hodges JT, Jacquemart D, Mlawer EJ, Nikitin AV, Perevalov VI, Rotger M, Tennyson J, Toon GC, Tran H, Tyuterev VG, Adkins EM, Baker A, Barbe A, Canè E, Császár AG, Dudaryonok A, Egorov O, Fleisher AJ, Fleurbaey H, Foltynowicz A, Furtenbacher T, Harrison JJ, Hartmann J-M, Horneman V-M, Huang X, Karman T, Karns J, Kassi S, Kleiner I, Kof-man V, Kwabia-Tchana F, Lavrentieva NN, Lee TJ, Long DA, Lukashchuk AA, Lyulin OM, Makhnev VY, Matt W, Massie ST, Melosso M, Mikhailenko SN, Mondelain D, Müller HSP, Naumenko OV, Perrin A, Polyansky OL, Raddaoui E, Raston PL, Reed ZD, Rey M, Richard C, Tóbiás R, Sadiek I, Schwenke DW, Starikova E, Sung K, Tamassia F, Tashkun SA, Vander Auwera J, Vasilenko IA, Viganin AA, Villanueva GL, Vispoel B, Wagner G, Yachmenev A, Yurchenko SN. The HITRAN2020 molecular spectroscopic database. *J Quant Spectrosc Radiat Transf* 2022;277:107949.
- [11] Delahaye T, Armante R, Scott NA, Jacquinet-Husson N, Chédin A, Crépeau L, Crevoisier C, Douet V, Perrin A, Barbe A, Boudon V, Campargue A, Coudert LH, Ebert V, Flaud JM, Gamache RR, Jacquemart D, Jolly A, Kwabia Tchana F, Kyuberis A, Li G, Lyulin OM, Manceron L, Mikhailenko S, Moazzen-Ahmadi N, Müller HSP, Naumenko OV, Nikitin A, IPerevalov V, Richard C, Starikova E, Tashkun SA, Tyuterev VLG, Vander Auwera J, Vispoel B, Yachmenev A, Yurchenko S. The 2020 edition of the GEISA spectroscopic database. *J Mol Spectrosc* 2021;380:111510.
- [12] Sharpe SW, Johnson TJ, Sams RL, Chu PM, Rhoderick GC, Johnson PA. Gas-phase Databases for Quantitative Infrared Spectroscopy. *Appl Spectrosc* 2004;58:1452-1461.
- [13] Dehayem-Kamadjeu A, Pirali O, Orphal J, Kleiner I, Flaud PM, The far-Infrared Rotational Spectrum of Nitrous Acid (HONO) and its Deuterated Species (DONO) studied by High-Resolution Fourier-Transform Spectroscopy. *J Mol Spectrosc* 2005;234:182–189.
- [14] Kleiner I, Guilmot JM, Carleer M, Herman M, The  $\nu_4$  Fundamental Bands of *trans*- and *cis*-HNO<sub>2</sub>. *J Mol Spectrosc* 1991;149:341–347.
- [15] Tchana Betnga W, Kwabia Tchana F, Perrin A, Manceron L, Vander Auwera J, Hindle F, Coutens A. New line intensities for the far infrared bands of the *trans*- and *cis*-conformer of nitrous acid (HONO), new determination of the *trans-cis* conformer barrier and its impact on the astrophysical detection of nitrous acid in protostellar clouds. *J Quant Spectrosc Radiat Transfer* 2023;310:108727.
- [16] Kagann RH, Maki AG. Infrared Absorption Intensities of Nitrous Acid (HONO) Fundamental Bands. *J Quant Spectrosc Radiat Transfer* 1983;30:37-44.
- [17] Sironneau V, Flaud JM, Orphal J, Kleiner I, Chelin P. Absolute line intensities of HONO and DONO in the far-infrared and re-determination of the energy difference between the *trans*- and *cis*-species of nitrous acid. *J Mol Spectrosc* 2010;259:100–104.
- [18] Richter F, Hochlaf M, Rosmus P, Gatti F, Meyer H.-D. A study of the mode-selective *trans-cis* isomerization in HONO using ab initio methodology *J. Chem. Phys.* 2004; 120: 1306- 1317. <https://doi.org/10.1063/1.1632471>

- [19] Allegrini M, Johns JWC, McKellar ARW, Pinson P. Stark spectroscopy with the CO Laser: the  $\nu_2$  fundamental bands of *trans*- and *cis*-nitrous acid, HNO<sub>2</sub>, in the 6  $\mu\text{m}$  region. *J Mol Spectrosc* 1980;79:446-454.
- [20] Tchana Betnga W, Hindle F, Manceron L, Vander Auwera J, Cuisset A, Mouret G, Bocquet R, Perrin A, Roy P, Kwabia Tchana F. A new instrumentation for simultaneous terahertz and mid-infrared spectroscopy in corrosive gaseous mixtures. *Review of Scientific Instruments* 2024;95:000000;doi: 10.1063/5.0178449.
- [21] Faye M, Bordessoule M, Kanouté B, Brubach JB, Roy P, Manceron L. Improved mid infrared detector for high spectral or spatial resolution and synchrotron radiation use. *Rev Sci Instrum* 2016;87:063119.
- [22] Syomin DA, Finlayson-Pitts B. HONO decomposition on borosilicate glass surfaces: implications for environmental chamber studies and field experiments. *Phys Chem Chem Phys* 2003;5:5236–5242.
- [23] Guinet M, Cuisset A, Croize L, Eliet S, Bocquet R, Hindle F. Versatile sub-THz spectrometer for trace gas analysis. *IEEE Sensors Journal* 2013;13:133–138.
- [24] Perrin A, Miljanic S, Dehayem-Kamadjeu A, Chélin P, Orphal J, Demaison J. The 14–22  $\mu\text{m}$  absorption spectrum of nitrous acid studied by high-resolution Fourier-transform spectroscopy: New analysis of the  $\nu_5$  and  $\nu_6$  interacting bands of *trans*-HONO and first analysis of the  $\nu_6$  band of *cis*-HONO. *J Mol Spectrosc* 2007;245:100–108.
- [25] Dore L. Using Fast Fourier Transform to compute the line shape of frequency-modulated spectral profiles. *J Mol Spectrosc* 2003;221:93-98.
- [26] Tudorie M, Foldes T, Vandaele AC, Vander Auwera J. CO<sub>2</sub> Pressure broadening and shift coefficients for the 1-0 band of HCl and DCl. *J Quant Spectrosc Radiat Transf* 2012;113:1092–101.
- [27] Daneshvar L, Foldes T, Buldyreva J, Vander Auwera J. Infrared absorption by pure CO<sub>2</sub> near 3340  $\text{cm}^{-1}$ : measurements and analysis of collisional coefficients and line-mixing effects at subatmospheric pressures. *J Quant Spectrosc Radiat Transf* 2014;149:258–74.
- [28] Wells R. Rapid approximation to the Voigt/Faddeeva function and its derivatives. *J Quant Spectrosc Radiat Transf* 1999;62:29–48.
- [29] Ballard J, Knight RJ, Vander Auwera J, Herman M, Di Lonardo G, Masciarelli G, Nicolaisen FM, Beukes JA, Christensen LK, McPheat R, Duxbury G, Freckleton R, Shine KP. An intercomparison of laboratory measurements of absorption cross-sections and integrated absorption intensities for HCFC-22. *J Quant Spectrosc Radiat Transf* 2000;66:109-28.
- [30] Fischer J, Gamache RR, Goldman A, Rothman LS, Perrin A. Total internal partition sums in the 2000 edition of the HITRAN database. *J Quant Spectrosc Radiat Transfer* 2003;82:401–412.

[31] Flaud JM, Camy-Peyret C, Toth RA. Water vapour line Parameters from microwave to medium Infrared (An atlas of  $\text{H}_2^{16}\text{O}$ ,  $\text{H}_2^{17}\text{O}$  and  $\text{H}_2^{18}\text{O}$  line positions and Intensities between 0 and  $4350\text{ cm}^{-1}$ ). 1<sup>st</sup> ed. Oxford: Pergamon Press; 1981.

[32] Shostak SL, Ebenstein WL, Muentzer JS. The dipole moment of water. I. dipole moments and hyperfine properties of  $\text{H}_2\text{O}$  and  $\text{HDO}$  in the ground and excited vibrational states. *J Phys Chem* 1991;94:5875–82.

### List of Tables

#### Table 1.

Total pressures in the equilibrium mixtures, derived partial pressures of HONO (in hPa) and number of interferograms averaged to yield the corresponding spectrum (# scans). All the IR spectra were recorded at a resolution of  $0.0021\text{ cm}^{-1}$  (equal to 0.9 divided by the maximum optical path difference), at  $294 \pm 1\text{ K}$ , an optical path length of 5.52 (2) m and an entrance aperture diameter of the interferometer equal to 1.7 mm. The uncertainty on the partial pressure of HONO takes into account the standard deviation from fit and the reading accuracy of 0.15% on the total pressure, according to the manufacturer's specification.

#	Total pressure in the mixture (hPa)	$P_{\text{HONO}}$ (hPa)	# Scans
S1	0.4105 (6)	0.00131 (2)	1840
S2	0.7155 (11)	0.00272 (5)	1910
S3	1.0151 (15)	0.00466 (10)	1230
S4	1.3126 (20)	0.00677 (17)	1830
S5	1.6052 (24)	0.00967 (26)	1870
S6	2.0525 (31)	0.01431 (47)	1870

**Table 2.**Results of the present assignment for the  $\nu_4$  bands of *trans*-HONO and *cis*-HONO

	<i>trans</i> -HONO	<i>cis</i> -HONO
Number of (non-degenerate lines)	1401	1863
Number of levels	785	825
$K_{a,\max}$	19	18
$J_{\max}$	55	61

**Table 3.**

Hamiltonian matrix

The  $\{5^1, 6^1, 4^1\}$  resonating states for *cis*-HONO

	$5^1$	$6^1$	$4^1$
$5^1$	$H_W$	Herm. conj	
$6^1$	$C^A + C^B$	$H_W$	Herm. conj
$4^1$		$C^B$	$H_W$

$$\begin{aligned}
H_W = & E_v + [A^v - 1/2 (B^v + C^v)]J_z^2 + 1/2 (B^v + C^v)J^2 + 1/2 (B^v - C^v)J_{xy}^2 \\
& - \Delta_K^v J_z^4 - \Delta_{JK}^v J_z^2 J^2 - \Delta_J^v (J^2)^2 - \delta_K^v \{J_z^2, J_{xy}^2\} - 2\delta_J^v J_{xy}^2 J^2 \\
& + H_K^v J_z^6 + H_{KJ}^v J_z^4 J^2 + H_{JK}^v J_z^2 (J^2)^2 + H_J^v (J^2)^3 \\
& + h_K^v \{J_z^4, J_{xy}^2\} + h_{KJ}^v \{J_z^2, J_{xy}^2\} J^2 + 2h_J^v J_{xy}^2 (J^2)^2 + \dots
\end{aligned}$$

$$C_{5^1 6^1}^A = C_{5^1 6^1}^{A,1} J_z + C_{5^1 6^1}^{A,2} \{iJ_y, J_x\} + C_{5^1 6^1}^{A,3} J_z J^2 \dots$$

$$C_{5^1 6^1}^B = C_{5^1 6^1}^{B,1} J_x + C_{5^1 6^1}^{B,2} \{iJ_y, J_z\} + C_{5^1 6^1}^{B,3} \{J_x, J_z^2\} \dots$$

$$C_{6^1 4^1}^B = C_{6^1 4^1}^{B,1} (J_-^3 - J_+^3).$$

with  $\{A, B\} = AB + BA$  and  $J_{xy}^2 = J_x^2 - J_y^2$  and  $J_{\pm} = J_x \pm iJ_y$

**Table 4.**

Vibrational band center, rotational and centrifugal distortion constants for the ground state [12] and for the  $4^1$  state of *trans*-HONO during this work and in Ref. [13].

	Ground state		$4^1$	
	Dehayem et al. [13]	This work #	Kleiner et al. [14]	
$E_v$		790.117130(18)	790.117045(32)	
A	3.09854472	3.118844849(900)	3.1188516(13)	
B	0.417788103	0.415681332(590)	0.41568013(21)	
C	$3.67476366 \times 10^{-1}$	0.364982889(540)	0.36498572(18)	
$\Delta_K$	$9.99541 \times 10^{-5}$	$1.0491138(730) \times 10^{-4}$	$1.04933(14) \times 10^{-4}$	
$\Delta_{JK}$	$1.72610 \times 10^{-6}$	$1.03277(130) \times 10^{-6}$	$1.0470(23) \times 10^{-6}$	
$\Delta_J$	$5.10440 \times 10^{-7}$	$5.007413(170) \times 10^{-7}$	$5.0192(16) \times 10^{-7}$	
$\delta_K$	$3.1076 \times 10^{-6}$	$3.45816(250) \times 10^{-6}$	$3.514(10) \times 10^{-6}$	
$\delta_J$	$6.8795 \times 10^{-8}$	$6.70838(110) \times 10^{-8}$	$6.5841(54) \times 10^{-8}$	
$H_K$	$1.0200 \times 10^{-8}$	$1.09882(150) \times 10^{-8}$	$1.0158(43) \times 10^{-8}$	
$H_{KJ}$	$-0.755 \times 10^{-9}$	$-1.18782(460) \times 10^{-9}$	$-0.7662 \times 10^{-9}$	
$H_{JK}$	$-6.29 \times 10^{-11}$	$-7.2120(440) \times 10^{-11}$	$-1.551(37) \times 10^{-10}$	
$H_J$	$-0.941 \times 10^{-12}$	$-1.22611(540) \times 10^{-12}$	$-1.081(46) \times 10^{-12}$	
$h_K$	$-0.109 \times 10^{-8}$		\$	$-7.78(26) \times 10^{-9}$
$h_{KJ}$	$-0.89 \times 10^{-11}$		\$	$-0.1464 \times 10^{-10}$
$L_K$	$-0.1144 \times 10^{-11}$		\$	0.

# The results are in  $\text{cm}^{-1}$  and the quoted uncertainties are one standard deviation.

\$The higher order centrifugal constants are fixed to those of the ground state values [13].

**Table 5.**

**Part A:** Vibrational band center, rotational and centrifugal distortion constants for the ground state [13] and for the  $4^1$  state of *cis*-HONO in Ref [14].

	Ground state		$4^1$
	Dehayem et al. [13]	Kleiner et al. [14]	
$E_v$			851.943054(32)
A	2.80533545		2.8250575(13)
B	0.439273052		0.43649429(22)
C	0.379067714		0.37562912(19)
$\Delta_K$	$6.53248 \times 10^{-5}$		$6.9756(16) \times 10^{-5}$
$\Delta_{JK}$	$-2.8796 \times 10^{-7}$		$-9.359(21) \times 10^{-7}$
$\Delta_J$	$5.68799 \times 10^{-7}$		$5.5755(17) \times 10^{-7}$
$\delta_K$	$2.82768 \times 10^{-6}$		$3.3894(85) \times 10^{-6}$
$\delta_J$	$9.36594 \times 10^{-8}$		$9.5281(55) \times 10^{-8}$
$H_K$	$5.397 \times 10^{-9}$		$5.388(62) \times 10^{-9}$
$H_{KJ}$	$-6.78 \times 10^{-10}$		$-7.340(96) \times 10^{-10}$
$H_J$	$-1.078 \times 10^{-10}$		0.
$h_K$	$1.262 \times 10^{-9}$		$1.174(52) \times 10^{-9}$
$h_{KJ}$	$-0.841 \times 10^{-11}$		$-0.6738 \times 10^{-9}$
$L_K$	$-0.428 \times 10^{-12}$		0.

*Note.* The results are in  $\text{cm}^{-1}$  and the quoted uncertainties are one standard deviation.

**Part B:** Vibrational band center, rotational and centrifugal distortion constants for the  $\{5^1, 6^1, 4^1\}$  interacting states of *cis*-HONO (this work).

	$5^1$	$6^1$	$4^1$
$E_v$	609.2262(17)	639.743309(94)	851.943054(32)
A	2.8031321(290)	2.79387439(310)	2.8250575(13)
B	0.43502101(860)	0.43479162(810)	0.43649429(22)
C	0.37486703(230)	0.377535790(680)	0.37562912(19)
$\Delta_K$	\$	$6.03252(130)\times 10^{-5}$	$6.983936(840)\times 10^{-5}$
$\Delta_{JK}$	\$	$+1.31661(440)\times 10^{-6}$	$9.5577(280)\times 10^{-7}$
$\Delta_J$	\$	$5.91839(330)\times 10^{-7}$	$5.593386(710)\times 10^{-7}$
$\delta_K$	\$	$2.0356(300)\times 10^{-6}$	$3.57720(480)\times 10^{-6}$
$\delta_J$	\$	$9.8508(240)\times 10^{-8}$	$9.39308(55)\times 10^{-8}$
$H_K$	\$	\$	$6.3202(230)\times 10^{-9}$
$H_{KJ}$	\$	\$	$8.338(110)\times 10^{-10}$
$H_J$	\$	\$	\$
$h_K$	\$	\$	$1.0742(550)\times 10^{-9}$
$h_{KJ}$	\$	\$	\$
$L_K$	\$	\$	\$

**Coupling constants**

$5^1 \leftrightarrow 6^1$	
$J_x$	$5.948(210)\times 10^{-2}$
$\{iJ_y, J_x\}$	$9.2287(300)\times 10^{-4}$
$\{iJ_y, J_z\}$	$3.219(170)\times 10^{-3}$
$\{iJ_y, J_x\} \mathbf{J}^2$	$-4.376(130)\times 10^{-8}$
$\{iJ_y, J_z\} \mathbf{J}^2$	$-5.0015(330)\times 10^{-7}$
$5^1 \leftrightarrow 6^1$	
$(J_-^3 - J_+^3)$	$1.7601(720) \times 10^{-6}$

*Note.* The results are in  $\text{cm}^{-1}$  and the quoted errors are one standard deviation. Constants marked with \$ were held fixed to the ground state values [13] during the least-squares fit.

**Table 6.**

Transition dipole moment constants for the  $\nu_4$  transition moment operators for *trans*-HONO and *cis*-HONO

		This work		Armante et al. [6]	
		<i>trans</i> -HONO <sup>(a)</sup>	<i>cis</i> -HONO <sup>(a)</sup>	<i>trans</i> -HONO <sup>(a)</sup>	<i>cis</i> -HONO <sup>(a)</sup>
$\varphi_x$	$\mu_1^B$	--	0.107291(970)		0.115
	$\mu_1^A$	0.287663(240)	0.353804(240)	0.256	0.332
1 $/2(\{\varphi_x, iJ_y\}$ $- \{i\varphi_y, J_x\})$	$\mu_4^A$	$0.1805(120) \times 10^{-3}$	$0.23025(960) \times 10^{-3}$		
$\Delta E_{\text{cis-trans}}^{(b)}$		$95.8 \pm 9.2 \text{ cm}^{-1}$ [15]		$143 \text{ cm}^{-1}$ [16]	

<sup>(a)</sup>Values in Debye (1 D =  $3.33564 \times 10^{-30}$  C.m) and the quoted uncertainties are one standard deviation.

<sup>(b)</sup>Values of  $\Delta E_{\text{cis-trans}}$  that were used for the  $\nu_4$  line intensity computations.

**Table 7.**

Statistical analysis for the line intensity computation.

Source	<i>trans</i> -HONO	<i>cis</i> -HONO
Number of lines:	452	568
$0 \leq \delta < 8 \%$	81.9 %	76.6 %
$8 \% \leq \delta < 10 \%$	3.8 %	5.5 %
$10 \% \leq \delta < 20 \%$	11.3 %	10.7 %
$20 \% \leq \delta < 40 \%$	3.0 %	7.2 %

$$\delta = (\text{Int}_{\text{Obs}} - \text{Int}_{\text{Calc}}) / \text{Int}_{\text{Obs}} \text{ in } \%$$

**Table 8.**

Results of the present line intensity and position computation at 296 K.

	Conformer		Type	Nb of lines	Band intensity <sup>(1)</sup>	$\sigma_{\text{Min}}^{(2)}$	$\sigma_{\text{Max}}^{(2)}$	
	<i>trans</i>	v <sub>4</sub> band	A-type	10027	1.411	691.12	903.46	
v <sub>4</sub> band			B-type	n.n.				
			<i>total</i>		10027	1.411		
	<i>cis</i>	v <sub>4</sub> band	A-type	10911	1.459			
			B-type	12776	0.135			
			<i>total</i>		23731	1.594	723.60	1004.78
			v <sub>6</sub> lines <sup>(4)</sup>	C- type <sup>(4)</sup>	253	$2.3 \times 10^{-4}$	744.84	951.24
			v <sub>5</sub> lines <sup>(4)</sup>	A-type <sup>(4)</sup>	14	$4.0 \times 10^{-5}$	764.75	930.52
				B-type <sup>(4)</sup>	12	$3.5 \times 10^{-6}$		
	<b>Total</b>			<b>33993</b>	<b>3.006</b>			

(1) Line intensities are given in  $10^{-17} \times \text{cm}^{-2}/(\text{molecule} \cdot \text{cm}^{-1})$  @ 296 K(2) Wavenumber range in  $\text{cm}^{-1}$ (3) The intensity threshold limit is  $0.5 \times 10^{-24} \times \text{cm}^{-2}/(\text{molecule} \cdot \text{cm}^{-1})$ (4) For Cis-HONO these forbidden  $\Delta K_a = 2$  or  $\Delta K_a = 3$  transitions from the v<sub>5</sub> and v<sub>6</sub> bands appear in the line list in the 11  $\mu\text{m}$  region just because of the existence of local resonances coupling the 4<sup>1</sup> energy levels with those of the strongly resonating {5<sup>1</sup>, 6<sup>1</sup>} energy levels.

**Table 9**

Test computations of the  $\nu_4$  band intensities for *trans*-HONO and *cis*-HONO at T=296 K and T=230 K, for different values of  $\Delta E_{\text{cis-trans}}$ .

$\Delta E_{\text{cis-trans}}^{(1)}$		$T_{\text{tot}}Z(T)$	Band intensity <sup>(2)</sup> Trans-HONO	Band intensity <sup>(2)</sup> Cis-HONO	Band intensity <sup>(2)</sup> Total HONO	Ratio cis/trans
95.8	T=296K	14305.2	1.411	1.594	3.006	1.1295
95.8	T=230K	8588.4	1.633	1.609	3.243	0.9855
86.	T=296K	14553.1	1.411 <sup>(3)</sup>	1.594 <sup>(3)</sup>	3.006 <sup>(3)</sup>	1.1295 <sup>(3)</sup>
	T=230K	8767.5	1.627	1.625	3.252	0.9982
105.	T=296K	14068.2	1.411 <sup>(3)</sup>	1.594 <sup>(3)</sup>	3.006 <sup>(3)</sup>	1.1295 <sup>(3)</sup>
	T=230K	8419.3	1.638316	1.5939669	3.232	0.9729

<sup>(1)</sup> Value of  $\Delta E_{\text{cis-trans}}$  (in  $\text{cm}^{-1}$ ) used for the different test calculations performed at T=296K and T=230K ( $\Delta E_{\text{cis-trans}} = 95.8 \pm 9.2 \text{ cm}^{-1}$ ).

<sup>(2)</sup>  $\nu_4$  band intensities for *trans*-HONO and *cis*-HONO in  $10^{-17} \times \text{cm}^{-2}/(\text{molecule} \cdot \text{cm}^{-1})$  @ T=296 K or T= 230 K.

<sup>(3)</sup> at 296 K our computed intensities differ marginally with  $\Delta E_{\text{cis-trans}}$  (see text).

## List of figures

**Figure 1.**

Overview spectra of the entire  $\nu_4$  bands of *trans*- and *cis*-HONO recorded using high-resolution Fourier-transform spectroscopy (resolution =  $0.0021\text{ cm}^{-1}$ , optical pathlength = 5.52 m, 294 K) at different total pressures of the mixtures. The distinctive shape of the A-type  $\nu_4$  bands of *trans*-HONO and *cis*-HONO with their narrow Q-branches are clearly recognizable.

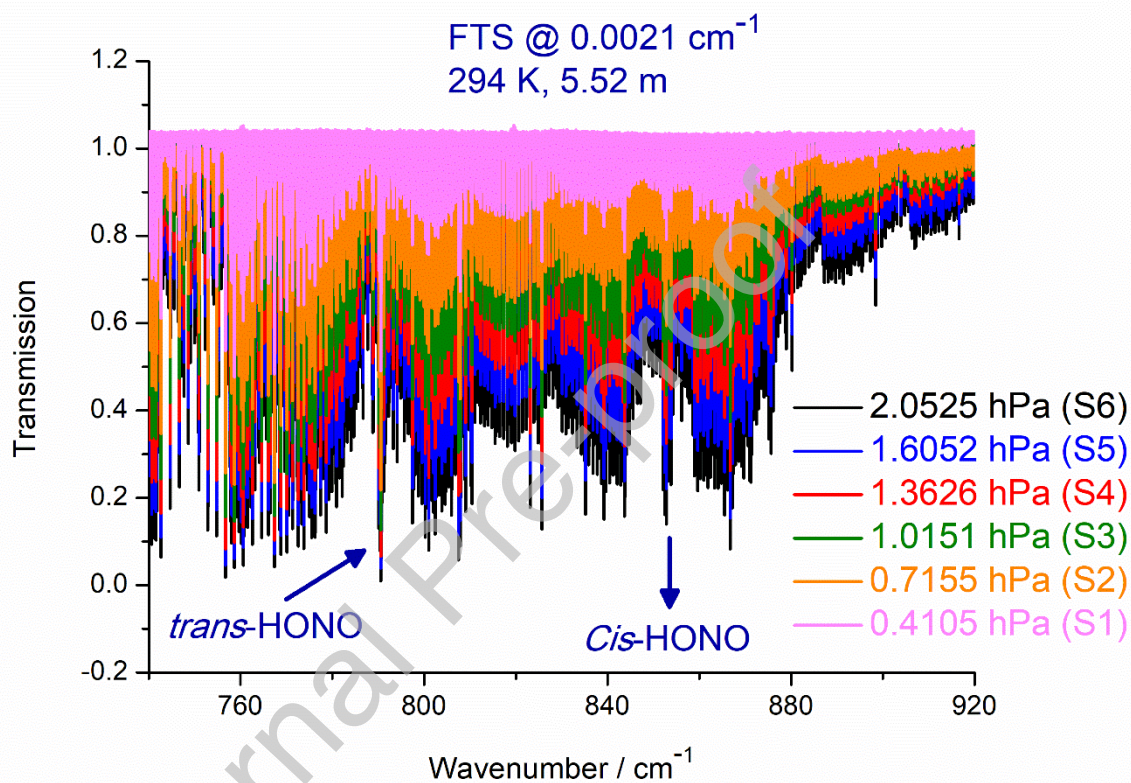


**Figure 2.**

Pure rotational transition ([16,0,16]-[15,1,15]) of *cis*-HONO at 361.821 GHz recorded at different total pressures of the mixtures, a 2F modulation frequency of 17.013 kHz and a modulation depth of 1080 kHz. The second harmonic signal is read in volts from the lock-in detection. Its value not only depends on the line profile and the modulation depth, but also the source power, detector responsivity, and amplifier settings. The response of a given experimental configuration can be easily calibrated by measuring the response of a stable gas with a well-known line strength.

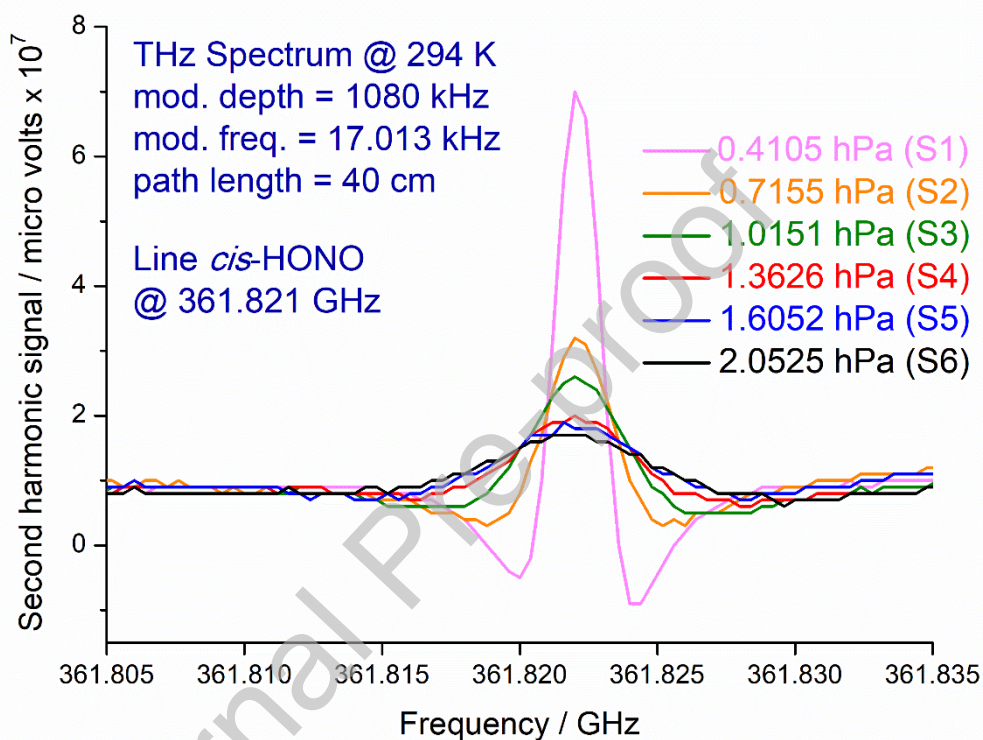


**Figure 3.**

Observed-Calculated energies for the  $K_a = 0$  levels of the  $4^1$  states of *trans*-HONO and *cis*-HONO.

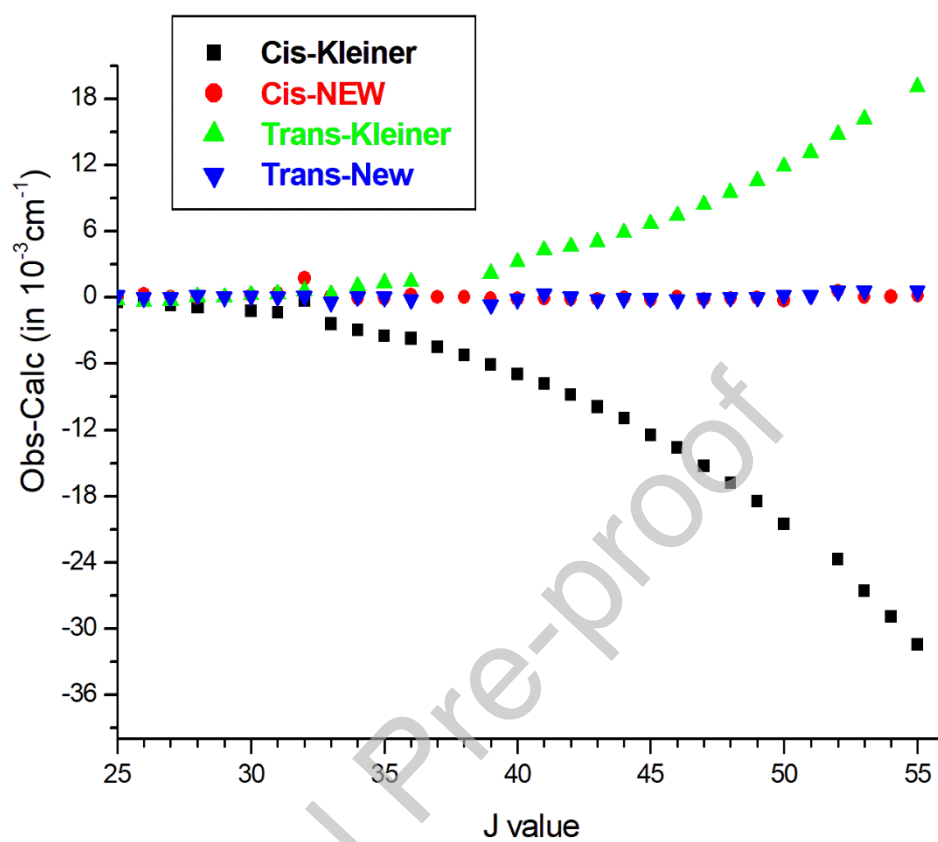


**Figure 4.**

Upper panel: pure rotation transition ([16,0,16]-[15,1,15]) of *cis*-HONO at 361821 MHz recorded at total pressure of 1.0151 hPa (S3), a modulation frequency of 17.013 kHz and a modulation depth of 1080 kHz (open circles) overlaid with the corresponding best-fit calculated spectrum (solid line) obtained using a Voigt profile as model line function; lower panel: percent differences between the observed and calculated spectra. The upper panel show the recorded THz signal, again this is the second harmonic signal but here it has been multiplied by  $10^7$  to aide its display.

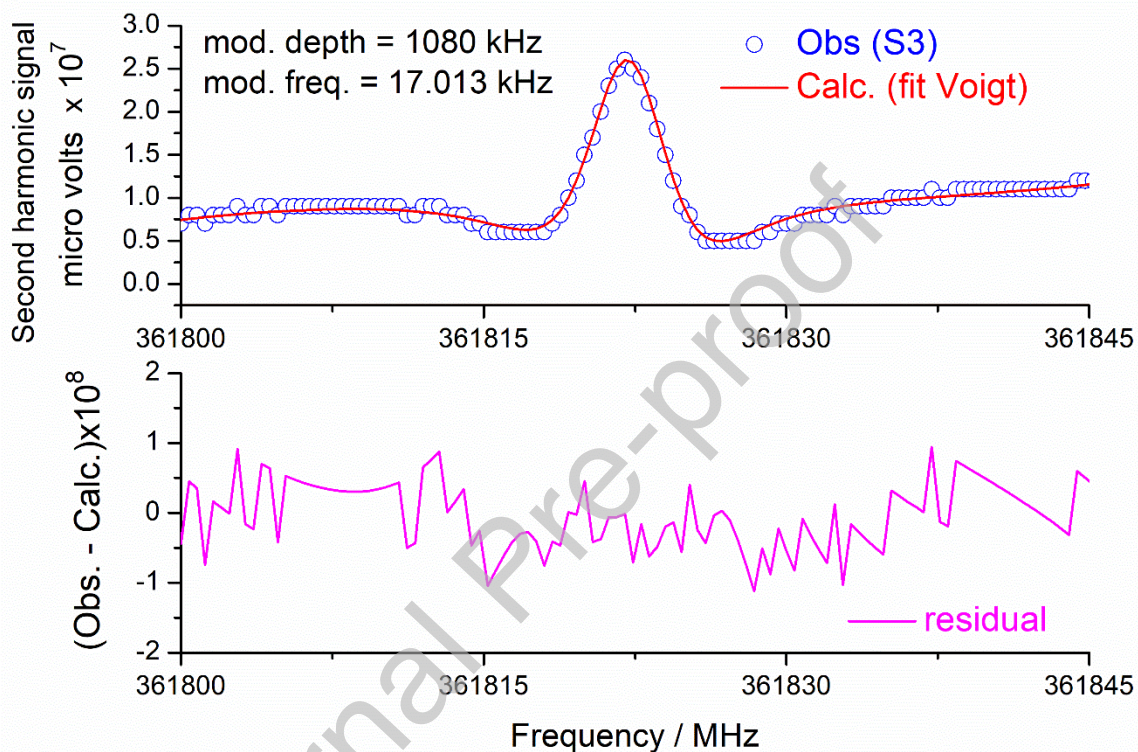


**Figure 5.**

Upper panel: small part of the spectrum of HONO lines (S2 in **Table 1**; open circles) overlaid by the corresponding best-fit calculated spectrum (solid line) obtained with a source aperture diameter of 1.7 mm, a maximum optical path difference of 428.57 cm and a Voigt profile; lower panel: percent differences between the observed and calculated spectra.

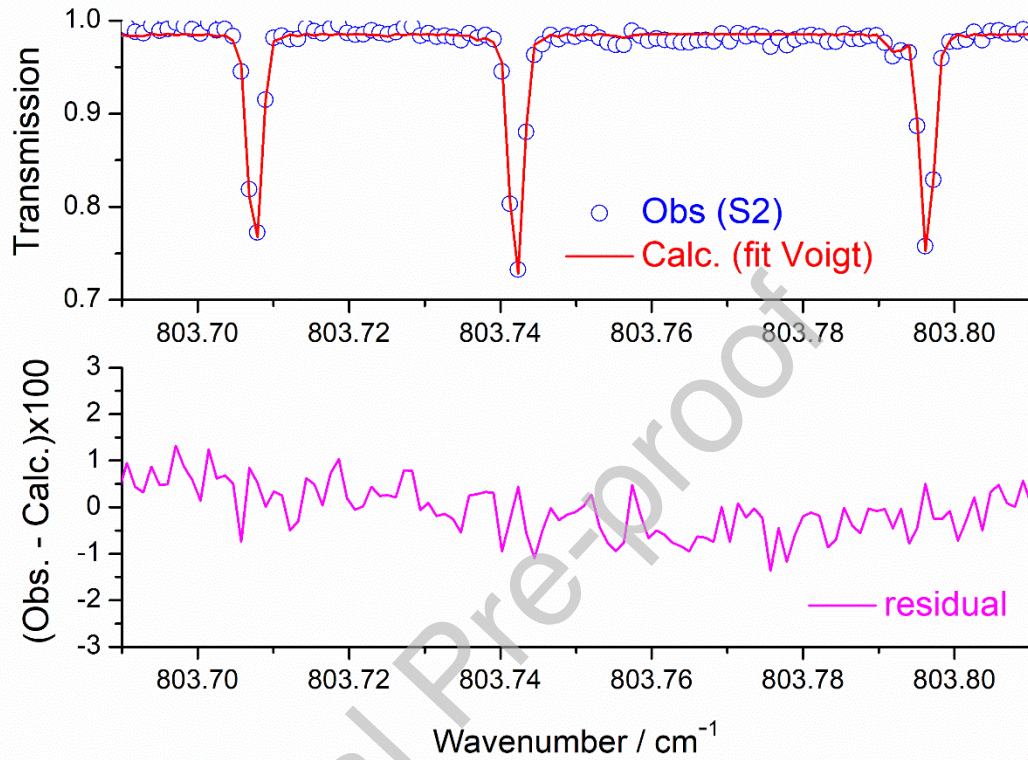


**Figure 6.**

Comparison between various sources of relative uncertainty on the measured intensities of 3 selected lines of high, medium and low intensity:  $Q_R(17,1)$ ,  $Q_R(14,10)$  and  $Q_P(16,12)$ .

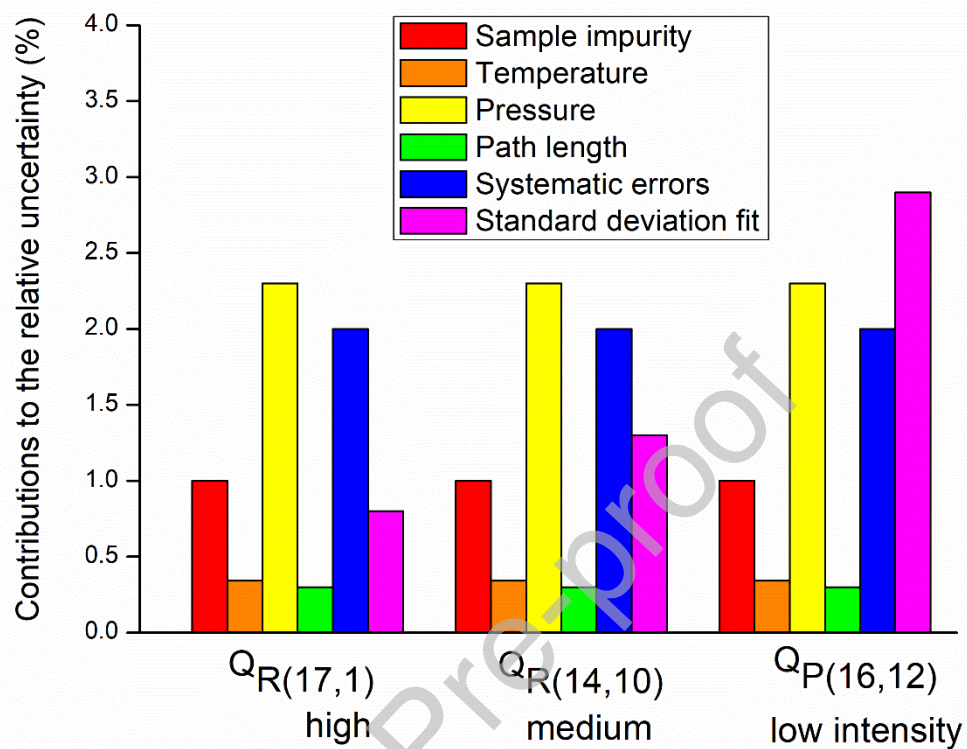


**Figure 7.**

Comparison between the PNNL absorption cross sections and the results of the present and “Old” [6] computations at  $T = 296$  K (upper panel). These computations are performed for HONO diluted in an atmosphere of nitrogen and for  $\gamma_{\text{Air}} = 0.1 \text{ cm}^{-1}/\text{atm}$ . For an easier relative comparison, both “New” and “Old” computed absorption cross sections are scaled artificially in intensity as (Calc\_New\_abs\_PNNL) and (Calc\_Old\_abs\_PNNL), relative to the PNNL values.

In the bottom panel, the difference (blue trace for “Old-New (abs\_PNNL)”) between these two computations, has a rather soft behavior at the resolution of the figure.

On the other hand, the (green) bottom trace that gives the difference between the PNNL (observed) and the “Calc\_New\_abs\_PNNL” calculated cross sections exhibits rather sharp signatures. Clearly neither computations account correctly for the probable line mixing effects in Q branch structures, or for the presence of hot bands in the PNNL cross sections.

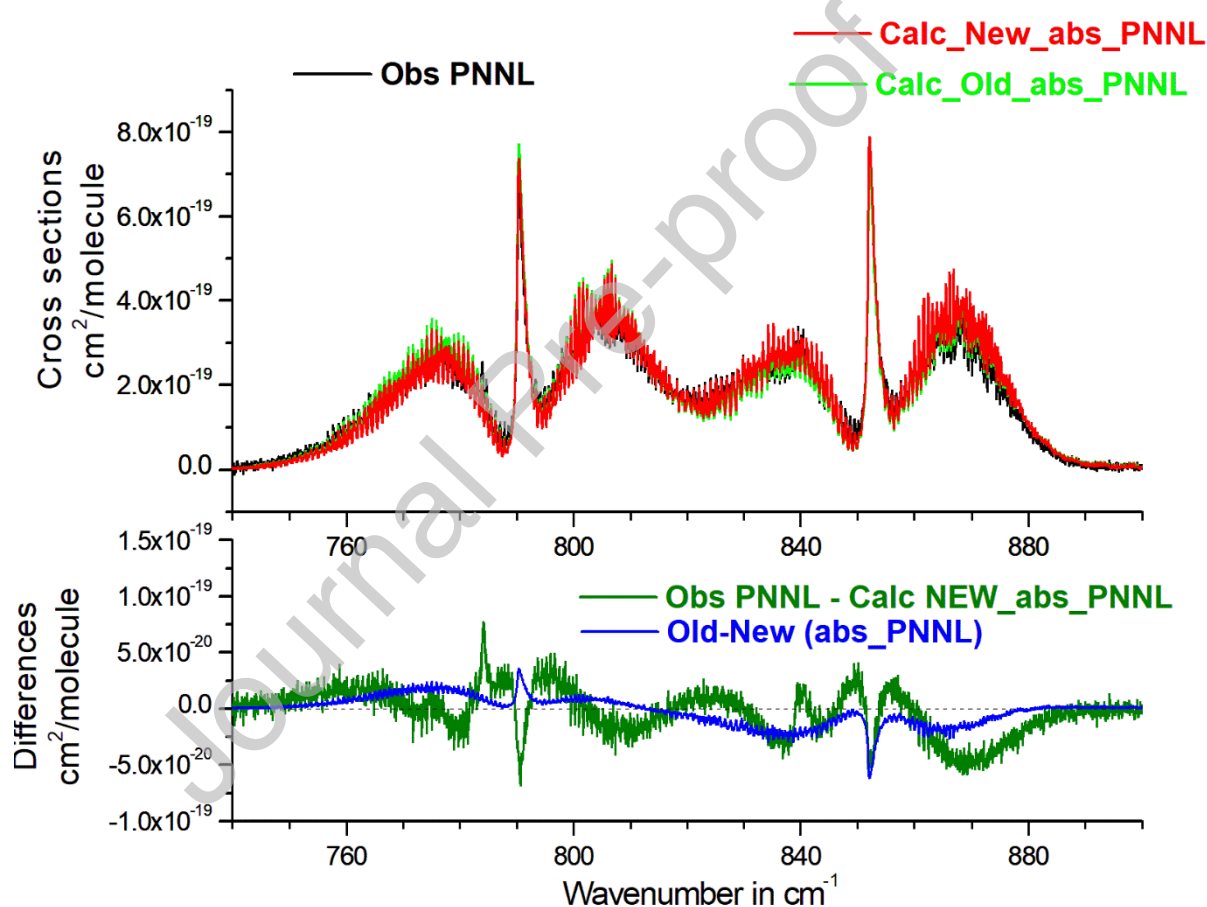


**Figure 8.**

Overview of the high resolution Fourier transform spectrum (S4) recorded during this work and comparison with the line by line spectra generated using the “New” line list and the “Old” one [6]. In this observed spectrum, the contributions due to CO<sub>2</sub> and NO<sub>2</sub> impurities are obvious. The intensities in the “Old” line list are, on the average, 24% weaker than the new ones. The bottom trace shows the difference, in positions, between the two line lists: \$ the overall intensities of the “Old” list are increased by 24%.

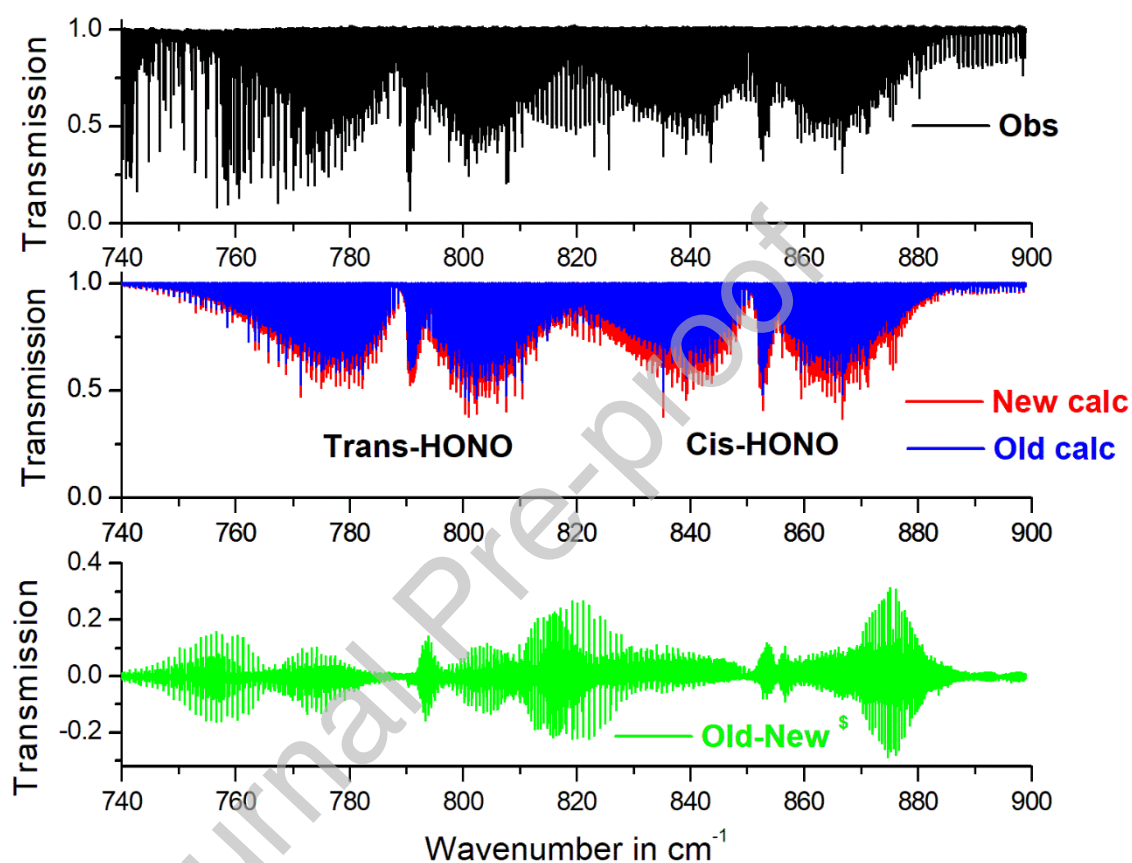


**Figure 9.**

Detailed view of the observed Fourier transform spectrum at  $755\text{ cm}^{-1}$ . The assignments are given for the  $[J, K_a, K_c]$  upper levels for P lines of *trans*-HONO. For very high  $K_c$  values ( $K_c \approx J$ ),  $K_a$  are degenerated ( $K_a = d$ ), and in this case the disagreement between the old computation and the observed lines is striking. The presence as impurity of  $\text{NO}_2$  impurity present in the cell during the spectra recording is evidenced by the lower trace.

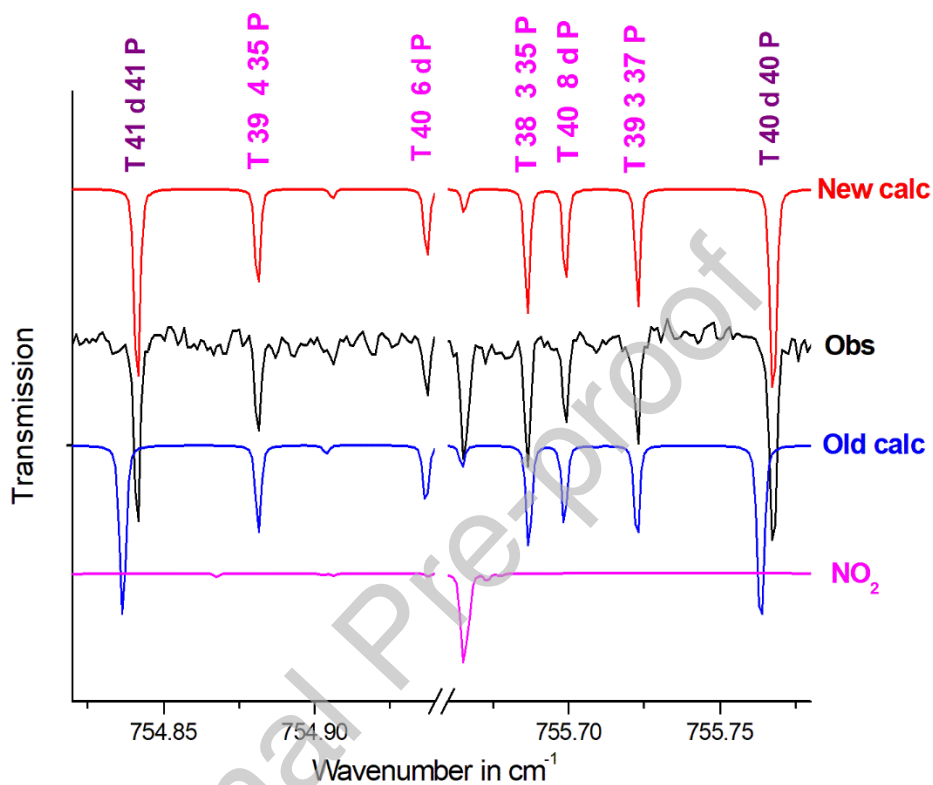


**Figure 10.**

Detailed view of the observed Fourier transform spectrum at  $795.5 \text{ cm}^{-1}$ . The assignments are given for the  $[J, K_a, K_c]$  upper levels, for Q lines or R lines of *trans*-HONO in the new and old calculation. Clearly, for  $K_a = 17$  (with  $K_c = d$  for degenerated), the positions of the “Old” line list differ from the observation.

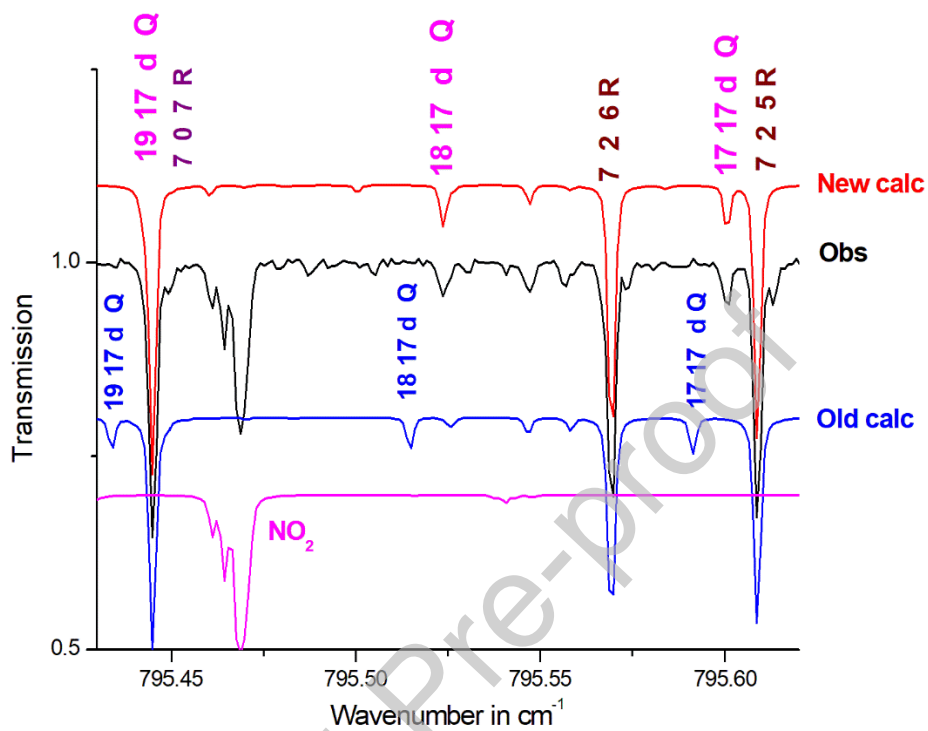


**Figure 11.**

Detailed view of the observed Fourier transform spectrum at  $816.2\text{ cm}^{-1}$ . The assignments are given for the  $[J, K_a, K_c]$  upper levels, for R lines of *trans*-HONO (with T letters) and P line of *cis*-HONO (with C letter). For very high  $K_c$  values ( $K_c \approx J$ ),  $K_a$  are degenerated ( $K_a = d$ ) and for these lines the positions of the “Old” line list differ from the observation.

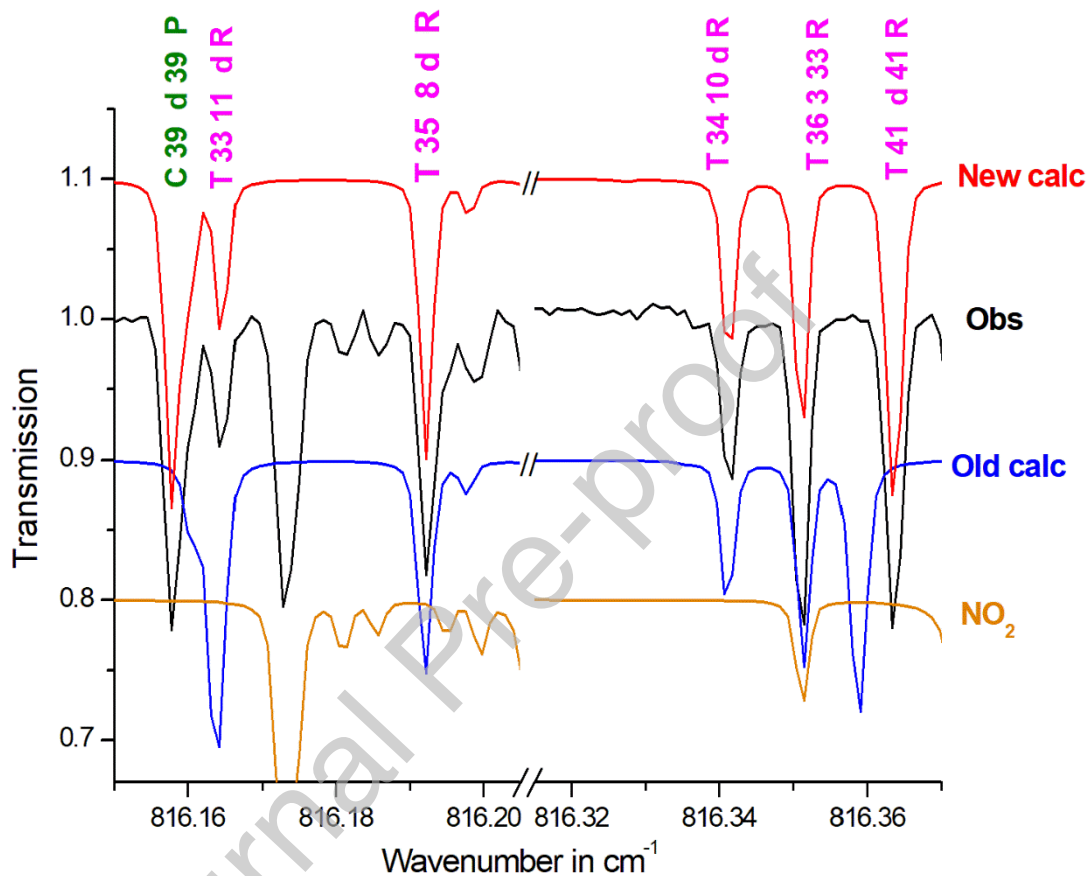


**Figure 12.**

Detailed view of the observed Fourier transform spectrum at  $877.5\text{ cm}^{-1}$ . The assignments are given for the  $[J, K_a, K_c]$  upper levels, for A-type ( $\Delta K_a = 0$ ) R lines of *cis*-HONO (with C letter). The  $K_a = d$  quoted for  $K_a = J - K_c$  and  $K_a = J - K_c + 1$  (resp.  $K_c = d$  quoted for  $K_c = J - K_a$  and  $K_c = J - K_a + 1$ ) are degenerated values. The largest differences between the observed and the “old” calculated positions are for the series involving very high  $K_c$  ( $K_a = d$ ) values. One individual B-type transition for *cis*-HONO is also observable (see \$).

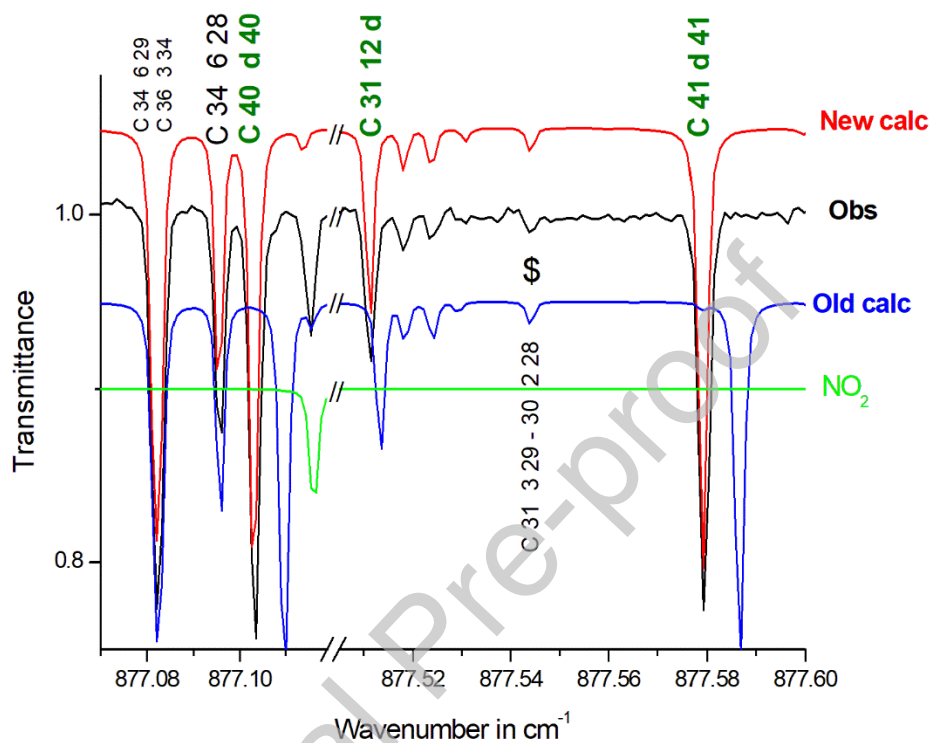
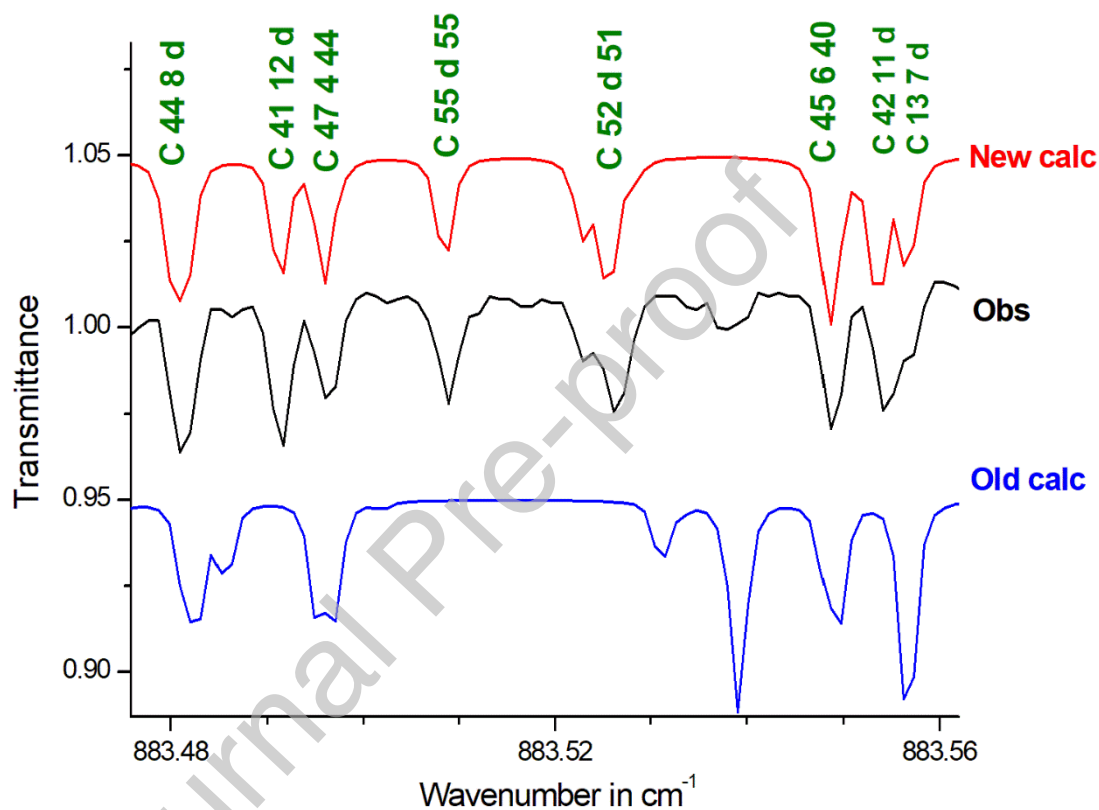


**Figure 13.**

Detailed view of the observed Fourier transform spectrum at  $883.5\text{ cm}^{-1}$ . The assignments are given for the  $[J, K_a, K_c]$  upper levels, for R lines of *cis*-HONO (with C letter). The  $K_a = d$  quoted for  $K_a = J - K_c$  and  $K_a = J - K_c + 1$  (resp.  $K_c = d$  quoted for  $K_c = J - K_a$  and  $K_c = J - K_a + 1$ ) are degenerated values. For several lines the positions of the “Old” linelist differ from the observation.



## Author Agreement Statement

We the undersigned declare that this manuscript is original, has not been published before and is

not currently being considered for publication elsewhere.

We confirm that the manuscript has been read and approved by all named authors and that there

are no other persons who satisfied the criteria for authorship but are not listed. We further confirm that the order of authors listed in the manuscript has been approved by all of us.

We understand that the Corresponding Author (Agnès Perrin [agnes.perrin@lmd.ipsl.fr](mailto:agnes.perrin@lmd.ipsl.fr)) is the sole contact for the Editorial process.

She is responsible for communicating with the other authors about progress, submissions of revisions and final approval of proofs

Signed by all authors as follows

W. Tchana Betnga : [Wilfried.Tchana@lisa.ipsl.fr](mailto:Wilfried.Tchana@lisa.ipsl.fr)

A. Perrin : [agnes.perrin@lmd.ipsl.fr](mailto:agnes.perrin@lmd.ipsl.fr)

L. Manceron : [laurent.manceron@synchrotron-soleil.fr](mailto:laurent.manceron@synchrotron-soleil.fr)

J. Vander Auwera : [jean.vander.auwera@ulb.be](mailto:jean.vander.auwera@ulb.be)

F. Hindle : [francis.hindle@univ-littoral.fr](mailto:francis.hindle@univ-littoral.fr)

A. Cuisset : [arnaud.cuisset@univ-littoral.fr](mailto:arnaud.cuisset@univ-littoral.fr)

G. Mouret : [gael.mouret@univ-littoral.fr](mailto:gael.mouret@univ-littoral.fr)

R. Bocquet : [robin.bocquet@univ-littoral.fr](mailto:robin.bocquet@univ-littoral.fr)

P. Roy : [pascale.roy@synchrotron-soleil.fr](mailto:pascale.roy@synchrotron-soleil.fr)

X. Landsheere : [landsheere@lisa.ipsl.fr](mailto:landsheere@lisa.ipsl.fr)

A. Voute : [alexandre.voute@lisa.ipsl.fr](mailto:alexandre.voute@lisa.ipsl.fr)

F. Kwabia Tchana : [fridolin.kwabia@lisa.ipsl.fr](mailto:fridolin.kwabia@lisa.ipsl.fr)

Author addresses:

W. Tchana Betnga<sup>1,2</sup>, A. Perrin<sup>3,\*</sup>, L. Manceron<sup>1,4</sup>, J. Vander Auwera<sup>5</sup>, F. Hindle<sup>2</sup>, A. Cuisset<sup>2</sup>, G. Mouret<sup>2</sup>, R. Bocquet<sup>2</sup>, P. Roy<sup>5</sup>, X. Landsheere<sup>1</sup>, A. Voute<sup>1,4</sup> and F. Kwabia Tchana<sup>1</sup>

<sup>1</sup> Université Paris Cité and Univ Paris Est Creteil, CNRS, LISA, F-75013 Paris, France

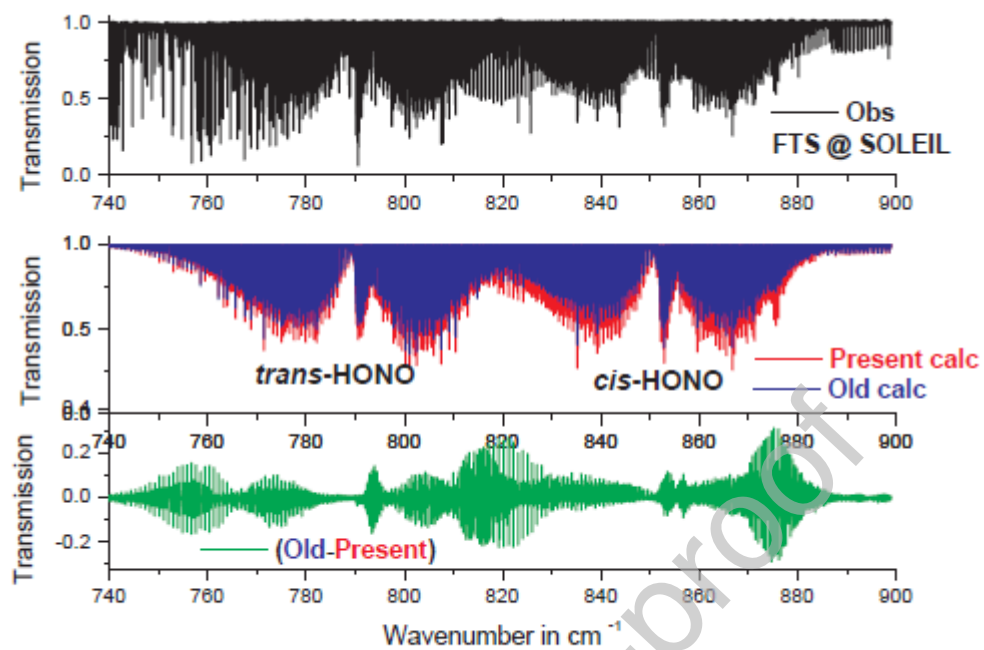
<sup>2</sup> Université du Littoral Côte d'Opale, UR 4493, Laboratoire de Physico-Chimie de l'Atmosphère, F-59140 Dunkerque, France

<sup>3</sup> Laboratoire de Météorologie Dynamique/IPSL, UMR CNRS 8539, Ecole Polytechnique, Université Paris-Saclay, RD36, 91128 Palaiseau Cedex, France

<sup>4</sup> Synchrotron SOLEIL, Ligne AILES, L'Orme des Merisiers, St-Aubin BP48, 91192 Gif-sur-Yvette Cedex, France

<sup>5</sup> Spectroscopy, Quantum Chemistry and Atmospheric Remote Sensing (SQUARES), C.P. 160/09, Université Libre de Bruxelles, 50 avenue F.D. Roosevelt, B-1050 Brussels, Belgium

## Graphical Abstract



**There is no conflict of interest.**

Hoping that this paper will be considered for publication in the Journal and looking forward to hearing from you, I remain,